ARTICLE

https://doi.org/10.1038/s41586-018-0321-x

Insights into clonal haematopoiesis from 8,342 mosaic chromosomal alterations

Po-Ru Loh[1,2,14]*, Giulio Genovese[2,3,4,14]*, Robert E. Handsaker[2,3,4], Hilary K. Finucane[2,5], Yakir A. Reshef[6], Pier Francesco Palamara[7], Brenda M. Birmann[8], Michael E. Talkowski[2,3,9,10], Samuel F. Bakhoum[11,12], Steven A. McCarroll[2,3,4,15]* & Alkes L. Price[2,13,15]*

The selective pressures that shape clonal evolution in healthy individuals are largely unknown. Here we investigate 8,342 mosaic chromosomal alterations, from 50 kb to 249 Mb long, that we uncovered in blood-derived DNA from 151,202 UK Biobank participants using phase-based computational techniques (estimated false discovery rate, 6–9%). We found six loci at which inherited variants associated strongly with the acquisition of deletions or loss of heterozygosity in *cis*. At three such loci (*MPL*, *TM2D3–TARSL2*, and *FRA10B*), we identified a likely causal variant that acted with high penetrance (5–50%). Inherited alleles at one locus appeared to affect the probability of somatic mutation, and at three other loci to be objects of positive or negative clonal selection. Several specific mosaic chromosomal alterations were strongly associated with future haematological malignancies. Our results reveal a multitude of paths towards clonal expansions with a wide range of effects on human health.

Clonal expansions of blood cells containing somatic mutations are often observed in individuals without cancer[1–13]. Consistent with the idea that clonal mosaicism can be a precancerous state, detectable mosaicism confers a more than tenfold increased risk of future haematological malignancy[1–4] and often involves pro-proliferative mutations. Several studies have suggested that inherited variation can influence the likelihood of clonal mosaicism[11,14–21].

The limiting factor in almost all studies of clonal mosaicism has been sample size, with earlier insights arising from analyses of up to around 1,000 mosaic events. Two key factors determine the number of detectable mosaic mutations: the number of individuals analysed, and the ability to detect clonal expansions present at low-to-modest cell fractions. Here we describe insights from an analysis of 8,342 mosaic chromosomal alterations (mCAs) which we identified in single nucleotide polymorphism (SNP) array data from 151,202 UK Biobank participants[22] using a sensitive algorithm we developed to make use of long-range haplotype phase information (building on published work[8]). We also draw upon data on health outcomes during 4–9 years after DNA sampling.

These data provide insights into clonal expansion, including mechanisms by which inherited variants at several loci act in *cis* to generate or propel mosaicism. We also identify specific mCAs that associate strongly with future haematological malignancies.

Mosaic chromosomal alterations in UK Biobank

We analysed allele-specific SNP-array intensity data previously obtained by genotyping blood-derived DNA from 151,202 UK Biobank participants (40–70 years of age)[22]; 607,525 genotyped variants remained after quality control (see Methods). We detected mCAs at cell fractions as low as 1% by using long-range phase information that is uniquely available in the UK Biobank[23,24]. Intuitively, accurate phasing allows the detection of subtle imbalances in the abundances of two haplotypes by combining allele-specific information across a very large number of SNPs (Extended Data Fig. 1). To make maximal use of phase information, we developed a new statistical method for phase-based mCA detection (see Methods and Supplementary Note 1).

We detected 8,342 mCAs (in 7,484 of the 151,202 individuals analysed) at an estimated false discovery rate (FDR) of 6–9% (Fig. 1, Extended Data Fig. 2, Supplementary Table 1, and Supplementary Notes 2, 3; validation rates could differ from this FDR estimate). We confidently classified 71% of the detected mCAs as either loss, copy-number neutral loss of heterozygosity (CNN-LOH), or gain; for the other 29% of events, copy-number state could not be inferred definitively (Fig. 2a and Supplementary Note 1). Most detected mCAs (5,901 of 8,342) were present at inferred cell fractions below 5% (Supplementary Note 4) and would have been undetectable without long-range phasing (Supplementary Note 5). The genomic distribution of detected mCAs was broadly consistent with those found in previous studies[1,2,7,8], as was the observation that individuals acquire multiple mCAs much more frequently than expected by chance (Fig. 2b, Extended Data Fig. 3, Supplementary Tables 2, 3, and Supplementary Note 6); differences (for example, in relative rates of del(20q) calls[25]) could be explained by differing methodological sensitivity or genotyping platforms (Supplementary Note 4).

Commonly deleted regions (CDRs) below 1 Mb in length may indicate haploinsufficient tumour-suppressor genes for which loss of one copy promotes cell proliferation[2]. Focal deletions most frequently targeted 13q14, *DNMT3A*, and *TET2*, as previously observed[2,8]; we further observed that most CNN-LOH events on 13q, 2p, and 4q spanned the same CDRs (Fig. 1 and Supplementary Note 7). We

[1]Division of Genetics, Department of Medicine, Brigham and Women's Hospital and Harvard Medical School, Boston, MA, USA. [2]Program in Medical and Population Genetics, Broad Institute of MIT and Harvard, Cambridge, MA, USA. [3]Stanley Center for Psychiatric Research, Broad Institute of MIT and Harvard, Cambridge, MA, USA. [4]Department of Genetics, Harvard Medical School, Boston, MA, USA. [5]Schmidt Fellows Program, Broad Institute of MIT and Harvard, Cambridge, MA, USA. [6]Department of Computer Science, Harvard University, Cambridge, MA, USA. [7]Department of Statistics, University of Oxford, Oxford, UK. [8]Channing Division of Network Medicine, Department of Medicine, Brigham and Women's Hospital and Harvard Medical School, Boston, MA, USA. [9]Center for Genomic Medicine, Massachusetts General Hospital, Boston, MA, USA. [10]Department of Neurology, Massachusetts General Hospital and Harvard Medical School, Boston, MA, USA. [11]Department of Radiation Oncology, Memorial Sloan Kettering Cancer Center, New York, NY, USA. [12]Sandra and Edward Meyer Cancer Center, Weill Cornell Medicine, New York, NY, USA. [13]Departments of Epidemiology and Biostatistics, Harvard T.H. Chan School of Public Health, Boston, MA, USA. [14]These authors contributed equally: Po-Ru Loh, Giulio Genovese. [15]These authors jointly supervised this work: Steven A McCarroll, Alkes L Price. *e-mail: poruloh@broadinstitute.org; giulio.genovese@gmail.com; mccarroll@genetics.med.harvard.edu; aprice@hsph.harvard.edu

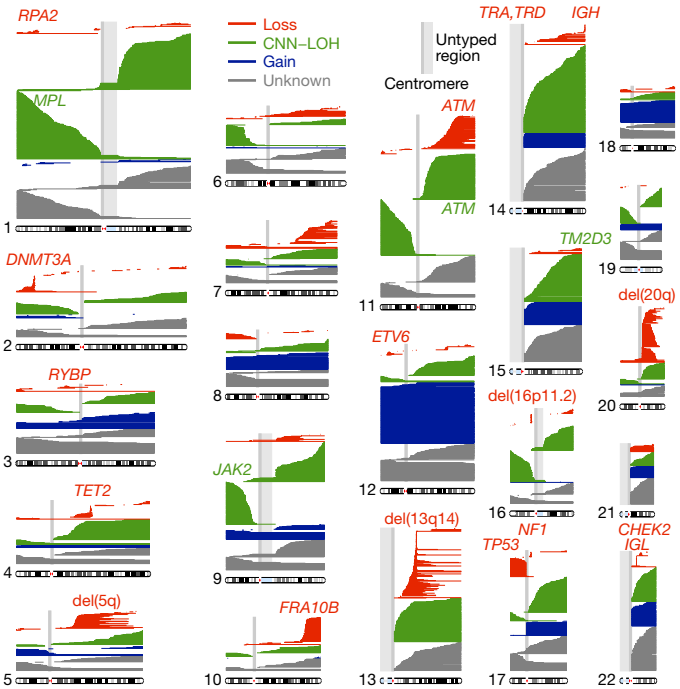

Fig. 1 | Mosaic chromosomal alterations detected in 151,202 UK Biobank participants. Each horizontal line corresponds to an mCA; a total of 5,562 autosomal events in 4,889 unique individuals are displayed. We detected an additional 2,780 chromosome X events in females (mostly whole-chromosome losses). Detected events are colour-coded by copy number. Focal deletions are labelled in red with names of putative target genes. Loci containing inherited variants influencing somatic events in *cis* are labelled in the colour of the mCA (red for del(10q)-associated *FRA10B*, green for CNN-LOH-associated loci). Enlarged per-chromosome plots are provided in Supplementary Note 2.

detected new CDRs at *ETV6*, *NF1*, and *CHEK2*, which are commonly mutated in cancers, and at *RPA2* and *RYBP*. We also detected a CDR at 16p11.2 overlapping a region whose deletion is a known risk factor for autism and other neuropsychiatric phenotypes, though we did not detect this mCA among 2,079 sequenced genomes from the Simons Simplex Collection (SSC)[26,27] (Supplementary Note 8). Deletions tended to be concentrated on chromosomes that are seldom duplicated[28] (Fig. 2c and Supplementary Table 1), supporting the theory that cumulative haploinsufficiency and triplosensitivity shape clonal evolution[29].

We found several notable exceptions to a general pattern in which acquired mutations are most common in the elderly and in males[1,2,7,8] (Fig. 2d and Supplementary Table 4). Loss of chromosome X in females[30] was by far the most common event we detected (Supplementary Table 1 and Supplementary Note 2), with frequency increasing markedly with advancing age (Fig. 2d and Supplementary Table 4). (We did not examine loss of chromosome Y, which has been studied elsewhere[21].) Stratification of autosomal mCAs by location and copy number revealed an unexpected relationship: although most gain events were (as expected) enriched in elderly individuals and in males, CNN-LOH events tended to affect both sexes equally (Fig. 2e and Supplementary Table 5). Three mCAs exhibited unusual age and sex distributions (FDR 0.05; binomial and *z*-tests): gains on chromosome 15 were much more frequent in elderly males[31]; and 16p11.2 deletions and 10q terminal deletions were much more frequent in females and exhibited frequency unrelated to age. Age-independent events could in principle occur early in development or take less time to reach high cell fractions; sex-specific effects (which we replicated in previous data sets[1,2,8]; Supplementary Note 3) will require future work to explain.

Some acquired mutations could in principle arise or be selected within specific haematopoietic lineages. We tested this hypothesis by examining individuals in the top percentile for counts of lymphocytes, basophils, monocytes, neutrophils, red blood cells, or platelets. We identified many mCAs that were significantly concentrated (FDR 0.05; Fisher's exact test) in one or more of these subsets of the cohort (Fig. 2f and Supplementary Table 6). Consistent with the idea that these relationships might reflect clonal selection in specific blood cell types, mutations commonly observed in chronic lymphocytic leukaemia (CLL)[32,33] were enriched among individuals with high lymphocyte counts, and *JAK2*-related 9p events (which are commonly observed in myeloproliferative neoplasms (MPNs)) were most common among individuals with high myeloid cell counts. While future work will be needed to replicate and further explore these findings, our results suggest that mCAs may produce blood-composition phenotypes in individuals with no known malignancy.

Inherited variants affect acquisition of nearby mCAs

To identify inherited influences on mCA formation or selection, we performed chromosome-wide scans for associations between mCAs and germline variants on the same chromosome (see Methods). This analysis revealed four loci at which inherited variation strongly associated with the acquisition of genomically nearby autosomal mCAs, and two loci on chromosome X associated with X loss in females (Table 1, Figs. 3, 4). We also replicated an earlier association of the *JAK2* 46/1 haplotype with 9p CNN-LOH[15–18,20] (Extended Data Fig. 4). To identify mechanisms that might underlie these associations, we fine-mapped these loci using whole-genome sequence (WGS) data and studied the phase of risk alleles relative to associated chromosomal alterations in *cis*.

Somatic terminal 10q deletions associated strongly ($P = 6.1 \times 10^{-42}$; Fisher's exact test) with the common SNP rs118137427 near *FRA10B*, a known genomic fragile site[34,35] at the estimated common breakpoint of the 10q deletions (Table 1 and Fig. 3a). All 60 individuals with these mosaic 10q deletions had inherited the rs118137427:G risk allele (the allele frequency is 5% in the population), which was always inherited on the same chromosome that subsequently acquired a terminal deletion (Table 1).

To identify a causal variant potentially tagged by the rs118137427:G risk allele, we searched for acquired 10q deletions in WGS data from 520 SSC families (see Methods). We identified two parent–child duos in which both parent and child had acquired the 10q terminal deletion (in mosaic form); all four individuals possessed expanded AT-rich repeats at *FRA10B* on the rs118137427:G haplotype background ($P = 0.01$; Fig. 3c). Further evidence that the rs118137427:G risk allele tags an unstable version of the *FRA10B* locus[36] was provided by analysis of the variable number tandem repeat (VNTR) sequence at *FRA10B* (in all 2,079 individuals). This analysis revealed a diversity of novel VNTR sequence motifs (12 distinct primary repeat units carried by 26 individuals from 14 families), all on the rs118137427:G haplotype background (Extended Data Fig. 5a, b and Supplementary Note 8). (The VNTR motifs did not associate with autism status in the SSC cohort.) The motifs had lengths of 38, 39, 42, and 43 bp and exhibited evidence of repeat expansion (probably more than 75 copies in the longest alleles[35]); by contrast, the hg19 reference sequence at *FRA10B* contains three copies of a 40-bp repeat. Imputing the VNTRs into the UK Biobank showed that they explained 24 of 60 del(10q) cases, despite being present in only about 0.7% of the cohort (Supplementary Table 7). Notably, individuals with del(10q) were as young as other UK Biobank participants, and 51 of 60 were female (binomial $P = 1.8 \times 10^{-7}$) (Fig. 3b); these unusual patterns (which were shared with 16p11.2 deletions) will require further study (Supplementary Note 8).

CNN-LOH events on chromosome (chr)1p strongly associated ($P = 6.2 \times 10^{-16}$, lead SNP rs144279563) with three independent, rare risk haplotypes (allele frequencies = 0.01–0.05%) at the *MPL* proto-oncogene at 1p34.1; the three haplotypes increased risk for 1p CNN-LOH by factors of 53, 63, and 103 (95% confidence intervals (CIs): 28–99, 29–139, and 35–300, respectively) (Table 1, Fig. 4a, and Supplementary Table 8). Other individuals with 1p CNN-LOH mosaicism also shared

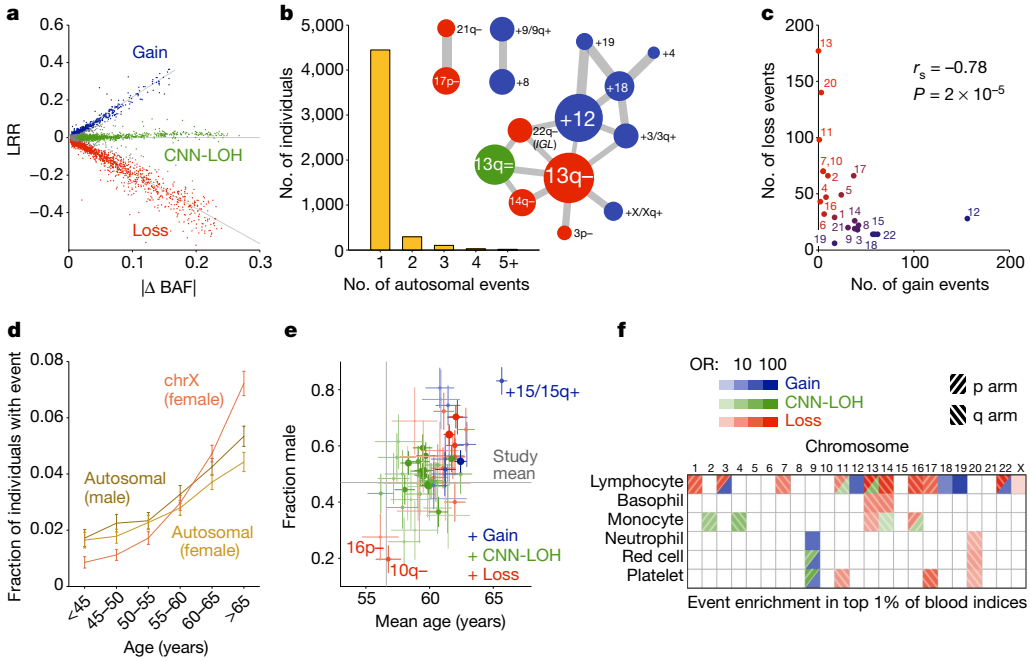

Fig. 2 | Distributional properties of detected mCAs. a, $\log_2 R$ ratio (LRR), measuring total allelic intensity, scales roughly linearly with B-allele frequency (BAF) deviation, measuring relative allelic intensity, among events with each copy number[1,2,8]. **b**, Most individuals with a detected autosomal mCA have only one event, although a larger number than expected (441 versus 100) have multiple events. Several pairs of mCA types co-occur much more frequently than expected by chance; edge weights in the co-occurrence graph scale with enrichment. **c**, Autosomes with more gain events tend to have fewer loss events (excluding deletions involving V(D)J recombination on chromosomes 14 and 22); Spearman's test on $n = 22$ autosomes. **d**, Fractions of individuals with at least one detected autosomal event increase steadily with age, and this trend is even more pronounced for X chromosome events in females. Error bars, 95% CI. **e**, Carriers of different mCA types have different age and sex distributions. Error bars, s.e.m. **f**, Different mCAs are significantly enriched (FDR 0.05) among individuals with anomalous blood counts in different blood lineages (adjusted for age, sex, and smoking status; see Methods). Numeric data including exact sample sizes used to compute error bars are provided in Supplementary Tables 1–6.

long haplotypes containing *MPL*, suggesting the existence of additional very rare risk variants (Extended Data Fig. 5c). Notably, although gain-of-function mutations in *MPL* lead to myeloproliferative neoplasms[37,38], the lead SNP on one haplotype, rs369156948, is a protein-truncating variant (PTV) in *MPL* with no association to haematological malignancies in the UK Biobank (0 cases among 36 carriers).

We were able to identify a likely mechanism for selection of the CNN-LOH events involving *MPL*. For all 16 events for which we could confidently phase the inherited risk allele relative to the somatic CNN-LOH, the CNN-LOH mutation had replaced the clonal haematopoiesis risk allele with the reference allele (binomial $P = 3 \times 10^{-5}$; Table 1 and Fig. 4a). These results suggest that, among individuals with rare inherited variants that reduce *MPL* function, recovery of normal *MPL* gene activity via CNN-LOH provides a proliferative advantage.

CNN-LOH events on chr11q associated ($P = 7.4 \times 10^{-9}$, OR = 41 (18–94)) with a rare risk haplotype (allele frequency = 0.07%)

Table 1 | Novel genome-wide significant associations of mCAs with inherited variants

						GWAS		Risk allelic shift in hets		
SV type	Locus	Variant	Location	Alleles[a]	RAF[b]	*P*	OR (95% CI)	N_{inc}[c]	N_{dec}[d]	*P*
***cis* associations**										
10q loss	*FRA10B*	rs118137427[e]	10q25.2	A/G	0.05	6.1×10^{-42}	18 (12–26)	0	43	2.3×10^{-13}
1p CNN-LOH	*MPL*	rs144279563	1p34.1	C/T	0.0005	6.2×10^{-16}	53 (28–99)	0	9	3.9×10^{-3}
		rs182971382	1p34.1	A/G	0.0003	3.0×10^{-11}	63 (29–139)	0	4	1.3×10^{-1}
		rs369156948[f]	1p34.2	C/T	0.0001	7.3×10^{-8}	103 (35–300)	0	3	2.5×10^{-1}
11q CNN-LOH	*ATM*	rs532198118	11q22.3	A/G	0.0007	7.4×10^{-9}	41 (18–94)	6	0	3.1×10^{-2}
15q CNN-LOH and loss	*TM2D3*, *TARSL2*	70 kb deletion[g]	15q26.3	CN = 1/0	0.0003	1.3×10^{-86}	698 (442–1102)	39	2	7.8×10^{-10}
chrX loss	*DXZ1*	rs2942875	Xp11.1	T/C	0.55	9.7×10^{-4}	1.09 (1.04–1.15)	423	796	6.6×10^{-27}
	DXZ4	rs11091036	Xq23	C/G	0.73	1.1×10^{-3}	1.10 (1.04–1.17)	369	555	1.0×10^{-9}
***trans* associations**										
chrX loss	*SP140L*	rs725201	2q37.1	G/T	0.56	9.2×10^{-10}	1.17 (1.12–1.24)			
	HLA	rs141806003	6p21.33	C/CAAAG	0.34	6.1×10^{-10}	1.18 (1.12–1.25)			

Results of two independent association tests are reported: a Fisher test treating individuals with a given mCA type as cases; and (for *cis* associations) a binomial test for biased allelic imbalance in heterozygous cases (hets; see Methods). All loci reaching $P < 1 \times 10^{-8}$ in either test are reported; each *cis* association detected by one test reached nominal ($P < 0.05$) significance in the other test. At significant loci, the lead associated variant as well as additional independent associations reaching $P < 1 \times 10^{-6}$ are reported.

[a]Risk-lowering/risk-increasing allele.

[b]Risk allele frequency (in UK Biobank participants with European ancestry).

[c]Number of mosaic individuals heterozygous for the variant in which the somatic event shifted the allelic balance in favour of the risk allele (by duplication of its chromosomal segment and/or loss of the homologous segment).

[d]Number of mosaic individuals heterozygous for the variant in which the somatic event shifted the allelic balance in favour of the non-risk allele.

[e]rs118137427 tags expanded repeats at *FRA10B* (Fig. 3).

[f]rs369156948 is a nonsense mutation in *MPL*.

[g]This deletion spans chr15:102.15–102.22Mb (hg19) and is tagged by rs182643535.

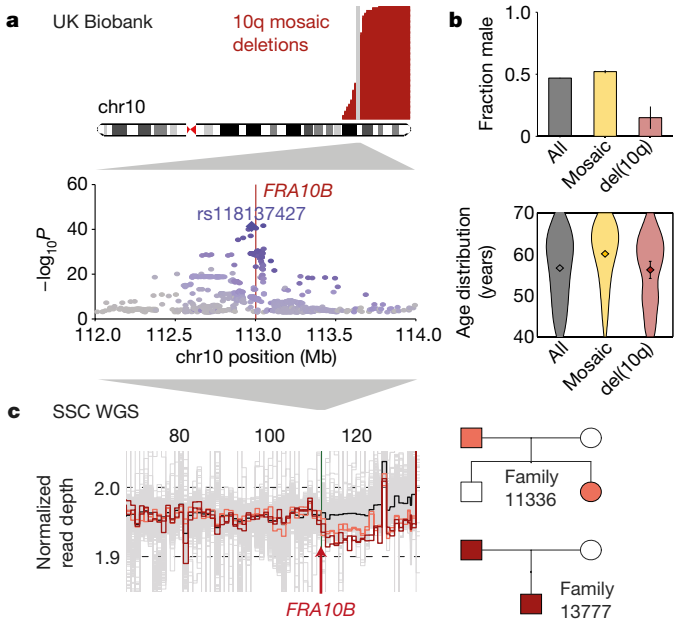

Fig. 3 | Repeat expansions at fragile site *FRA10B* driving breakage at 10q25.2. a, Germline variants at 10q25.2 associate strongly with terminal 10q mosaic deletion (Fisher's exact test, $n = 120{,}664$ individuals). Left boundaries of the deletions are called with error; true breakpoints are probably near-identical (Supplementary Note 4). **b**, UK Biobank carriers of terminal 10q deletion are predominantly female (top; 51 of $n = 60$ individuals; error bars, 95% CI) with age distribution similar to the overall study population (bottom; violin plot centres, means; error bars, 95% CI). **c**, WGS samples with terminal 10q deletion (two parent–child duos; right) carry inherited expanded repeats at *FRA10B*.

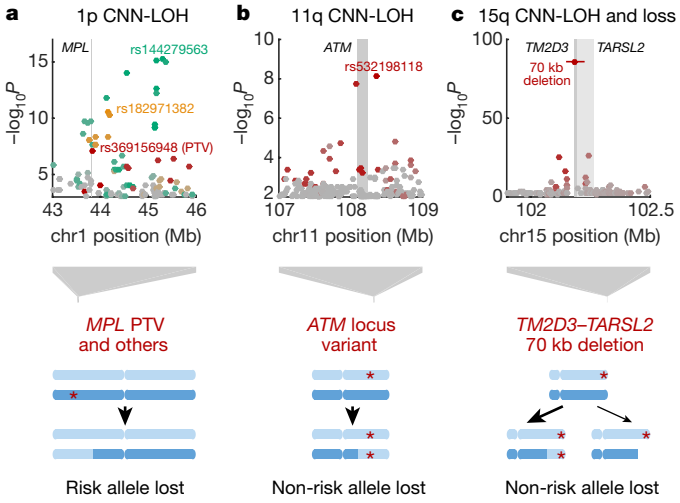

Fig. 4 | Novel loci associated with mCAs in *cis* due to clonal selection. **a**, *MPL*. **b**, *ATM*. **c**, *TM2D3–TARSL2*. In each locus, one or more inherited genetic variant predisposes chromosomal mutations to create a proliferative advantage. Bottom, genomic modifications; top, association *P* values (Fisher's exact test, $n = 120{,}664$ individuals). Independent lead associated variants are labelled, and variants are coloured according to linkage disequilibrium (LD) with lead variants (in shades of red, gold, or green; variants in grey are not in LD with lead variants). In **c**, the differing arrow weights to CNN-LOH and loss events indicate that CNN-LOH is the more common scenario (both in the population and among carriers of the risk variant).

surrounding the *ATM* gene at 11q22.3 (Table 1, Fig. 4b, and Supplementary Table 8). For all six CNN-LOH events for which we could confidently phase the risk allele relative to the somatic mutation, the LOH mutation had caused the rare risk allele to become homozygous, suggesting that the risk allele confers a proliferative advantage in the homozygous state (Table 1 and Fig. 4b). (This dynamic contrasts with that of *MPL*, at which the rare, inherited risk haplotypes were eliminated by LOH and clonal selection.) While sequencing would be required to identify a causal variant, *ATM* is a clear putative target: *ATM* encodes a DNA-damage response kinase that promotes DNA repair and limits cell division, and *ATM* is often inactivated by mutation in cancers[32,33]. In our analysis, acquired 11q deletions also appeared to target *ATM* (Fig. 1 and Supplementary Note 2).

CNN-LOH and loss events at chr15q associated strongly ($P = 1.3 \times 10^{-86}$) with a rare, inherited 70-kb deletion (allele frequency = 0.03%) that spanned all of *TM2D3* and part of *TARSL2* at 15q26.3 (Table 1, Fig. 4c, and Extended Data Figs. 6, 7). For 39 of 41 events with high-confidence phase calls, the CNN-LOH or loss was inferred to produce homozygosity or hemizygosity of the inherited deletion, removing the reference (non-deletion) allele from the genome. (This dynamic resembles that of *ATM* in suggesting clonal selection for the rare, inherited risk allele.) The 70-kb deletion increased risk of 15q mosaicism by a factor of 698 (442–1,102): 45 of 89 carriers exhibited detectable 15q events (32 CNN-LOH, 2 loss, 11 ambiguous between CNN-LOH and loss). Notably, the 70-kb deletion was sometimes inherited on an allele that also had an independent 290-kb duplication of the locus (Extended Data Fig. 6); on this more complex allele, *TM2D3* and *TARSL2* gene dosage were normal. Carriers of the more complex allele did not exhibit predisposition to mCAs. Further study will be required to determine a proliferative mechanism involving *TM2D3*, *TARSL2*, or noncoding elements within the region.

The high penetrances (up to 50%) for the above *cis* associations led us to suspect that some risk-allele carriers might harbour multiple subclonal cell populations with the associated alterations. Using a modified version of our methodology, we detected 39 individuals who had acquired two or more CNN-LOH mutations (with different breakpoints and allelic fractions) involving the same chromosome (Extended Data Fig. 8 and Supplementary Note 1). For all 39 individuals with multiple same-chromosome CNN-LOH events, all events involved recurrent selection of the same haplotype (in different clones). Of these 39 haplotypes, 16 carried a risk allele identified by our association scans, 13 appeared to involve other (undiscovered) alleles at the same loci, 5 duplicated 13q14 deletions, and 5 involved other genomic loci (Extended Data Fig. 8). This result indicates strong proliferative advantage conferred by CNN-LOH in these individuals and suggests that mitotic recombination occurs sufficiently frequently to yield multiple opportunities for clonal selection in individuals carrying inherited haplotypes with different proclivities for proliferation.

We also found two common variants on chromosome X that weakly increase risk of X loss while strongly influencing (in heterozygous females) which X chromosome is lost in the expanded clone. These involved a strong association ($P = 6.6 \times 10^{-27}$, 1.9:1 bias in the lost haplotype) at Xp11.1 near *DXZ1* and a weaker association ($P = 1.0 \times 10^{-9}$, 1.5:1 bias in the lost haplotype) at Xq23 near *DXZ4* (Table 1, Supplementary Table 9, and Supplementary Note 9). These associations do not appear to be explained by biased X chromosome inactivation[39] (Supplementary Table 10) and hint at yet another mechanism, different from those we have described.

Trans associations with mCAs

Genetic variants near genes involved in cell proliferation and cell cycle regulation predispose for male loss of Y[19,21], and female loss of X is also heritable ($h^2 = 26\%$ (17.4–36.2%) in sib-pair analysis)[21], but no associations for X loss have previously been reported, to our knowledge. We confirmed the heritability of female X loss by performing BOLT-REML[40] analysis (see Methods), obtaining a SNP-heritability estimate of $h_g^2 = 10.6\%$ (s.e. 3.6%). Genome-wide association analysis for *trans* variants influencing X loss further revealed two genome-wide significant associations at the *SP140L* and HLA loci (Table 1).

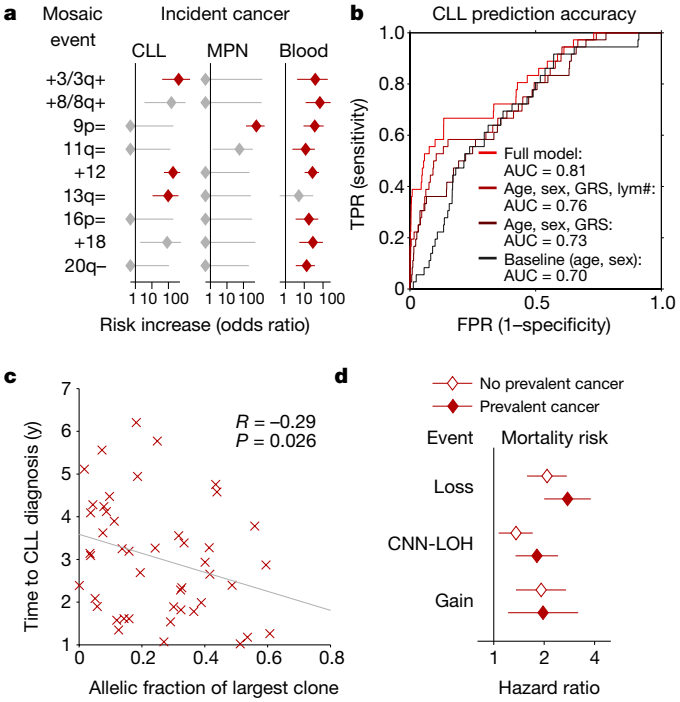

Fig. 5 | Associations between mCAs and incident cancers and mortality. **a**, Multiple mCA types confer increased risk of incident blood cancers diagnosed >1 year after DNA collection in $n = 109{,}819$ individuals with normal blood counts at assessment (Cochran-Mantel-Haenszel test adjusting for age and sex; error bars, 95% CI). **b**, A logistic model including mosaic status for 13q and trisomy 12 events along with other risk factors achieves high out-of-sample prediction accuracy for incident CLL ($n = 36$ cases and 113,923 controls with no cancer history). Lym#, log lymphocyte count. **c**, Time to malignancy tracks inversely with clonal cell fraction in $n = 46$ individuals with detectable clonality (of any mCA) who were diagnosed with CLL after assessment (one-sided Pearson's test). **d**, Loss, gain, and CNN-LOH events (on any autosome) all confer increased mortality risk in $n = 128{,}854$ individuals with no cancer history and $n = 15{,}782$ with prevalent cancers (error bars, 95% CI). Sample exclusions are detailed in the Methods. Numeric data are provided in Supplementary Tables 12 and 13.

Germline variants affecting cancer risk or chromosome-maintenance phenotypes could in principle increase the risk of clonal expansions. We considered 86 variants that have been implicated in previous genome-wide association studies (GWAS) on CLL, MPN, Y loss, clonal haematopoiesis, and telomere length and tested these variants for *trans* association with seven classes of mCAs, stratifying events by copy number and by autosome versus X chromosome. Four variants reached Bonferroni significance ($P < 8.3 \times 10^{-5}$): two linked variants in *TERT*[11,20,41], a rare frameshift mutation in *CHEK2*[20], and a low-frequency 3′ untranslated region (UTR) SNP in *TP53*[21,42] (Supplementary Table 11). The *TERT* and *CHEK2* variants associated with multiple types of autosomal event; by contrast, the *TP53* SNP primarily associated with losses (both focal autosomal deletions and X losses). Carriers of the *CHEK2* frameshift mutation were especially prone to developing multiple mCAs (one-sided binomial $P = 0.008$): 8 of 33 carriers with detected autosomal mosaicism had two or more mCAs, generally in multiple clones.

Mosaic chromosomal alterations and subsequent health

Cancer-free individuals with detectable mosaicism (at any locus) have a more than tenfold elevated risk of subsequent haematological cancer[1–4]. For CLL, a slowly progressing cancer that is known to be preceded by clonal mosaicism years before progression[43,44], mosaic alterations observed in patients who go on to develop CLL occur at the same loci as those observed in patients with CLL[32,33,45,46]. Using data on health outcomes for UK Biobank participants 4–9 years (median 5.7 years) after DNA sampling, we identified nine specific mCAs that were significantly associated (FDR 0.05) with subsequent haematological cancer diagnoses (more than 1 year after DNA collection) in analyses corrected for age and sex and restricted to individuals with normal blood counts at assessment (Fig. 5a and Supplementary Table 12), confirming and providing additional resolution to previous findings[1,2]. A logistic model combining mosaic status for CLL-associated events with other risk factors—age, sex, CLL genetic risk score[47], and lymphocyte count—achieved high CLL prediction accuracy (area under the curve (AUC) = 0.81) in tenfold cross-validation (Fig. 5b and Extended Data Fig. 9). Most of this predictive power came from early clones with trisomy 12, which we could detect at very low cell fractions (Extended Data Figs. 9, 10). Individuals with incident CLL exhibited clonality up to six years before diagnosis, and clonal fraction inversely correlated with time to malignancy (Fig. 5c). We further observed that detectable mosaicism roughly doubled risk for all-cause mortality (corrected for age, sex, and smoking status). This association was explained only partly by cancer deaths (Fig. 5d and Supplementary Table 13) and could reflect effects on cardiovascular illness[12], although further study is needed to explore this finding and rule out residual confounding.

Discussion

Mosaicism typically results from mutation followed by selective proliferation[10], and our results uncover diverse biological mechanisms underlying this transformation. We identified very rare inherited variants that affect either the likelihood of mutation (at *FRA10B*) or its proliferative impacts (due to CNN-LOH in *cis*), and we also observed *trans* influences on clonal haematopoiesis in the cell cycle genes *TP53*, *CHEK2*, and *TERT*. Our findings of *cis* risk loci for CNN-LOH expansions are particularly noteworthy: while some CNN-LOH expansions have previously been observed to provide a second hit to a frequently mutated locus[48] or to disrupt imprinting[49], here we observed that CNN-LOHs can also achieve strong selective advantage by duplicating or removing inherited alleles. The high penetrances (up to 50%) of the inherited CNN-LOH risk variants we identified challenge what is usually seen as a fundamental distinction between inherited alleles and (more capricious) acquired mutations. A large fraction of carriers of the inherited alleles subsequently acquire and then clonally amplify the mutations in question. The high penetrances imply that mitotic recombination is sufficiently common to predictably unleash latent, inherited opportunities for clonal selection of homozygous cells during the lifespan of an individual, corroborating a recent observation of this phenomenon in skin[50]. Similarly, we observed Mendelian inheritance patterns for 10q breakage at *FRA10B*, despite this event involving an acquired mutation.

Clonal expansions exhibit varying levels of proliferation and biological transformation and thus have a spectrum of effects on health[10]. We found that many mCAs, including some of those driven by *cis*-acting genetic variation, had no discernible adverse effects. However, mCAs commonly seen in blood cancers strongly increased cancer risk and could potentially be used for early detection—although we caution that these results are based on relatively short follow-up (4–9 years of cancer outcomes) and need independent replication. As population-scale efforts to collect genotype data and health outcomes continue to expand—increasing both sample sizes and the power of population-based chromosomal phasing—we anticipate ever-more-powerful analyses of clonal haematopoiesis and its clinical sequelae.

Online content

Any Methods, including any statements of data availability and Nature Research reporting summaries, along with any additional references and Source Data files, are available in the online version of the paper at https://doi.org/10.1038/s41586-018-0321-x.

Received: 2 August 2017; Accepted: 16 May 2018;
Published online: 11 July 2018

1. Jacobs, K. B. et al. Detectable clonal mosaicism and its relationship to aging and cancer. *Nat. Genet.* **44**, 651–658 (2012).
2. Laurie, C. C. et al. Detectable clonal mosaicism from birth to old age and its relationship to cancer. *Nat. Genet.* **44**, 642–650 (2012).
3. Genovese, G. et al. Clonal hematopoiesis and blood-cancer risk inferred from blood DNA sequence. *N. Engl. J. Med.* **371**, 2477–2487 (2014).
4. Jaiswal, S. et al. Age-related clonal hematopoiesis associated with adverse outcomes. *N. Engl. J. Med.* **371**, 2488–2498 (2014).
5. Xie, M. et al. Age-related mutations associated with clonal hematopoietic expansion and malignancies. *Nat. Med.* **20**, 1472–1478 (2014).
6. McKerrell, T. et al. Leukemia-associated somatic mutations drive distinct patterns of age-related clonal hemopoiesis. *Cell Reports* **10**, 1239–1245 (2015).
7. Machiela, M. J. et al. Characterization of large structural genetic mosaicism in human autosomes. *Am. J. Hum. Genet.* **96**, 487–497 (2015).
8. Vattathil, S. & Scheet, P. Extensive hidden genomic mosaicism revealed in normal tissue. *Am. J. Hum. Genet.* **98**, 571–578 (2016).
9. Young, A. L., Challen, G. A., Birmann, B. M. & Druley, T. E. Clonal haematopoiesis harbouring AML-associated mutations is ubiquitous in healthy adults. *Nat. Commun.* **7**, 12484 (2016).
10. Forsberg, L. A., Gisselsson, D. & Dumanski, J. P. Mosaicism in health and disease — clones picking up speed. *Nat. Rev. Genet.* **18**, 128–142 (2017).
11. Zink, F. et al. Clonal hematopoiesis, with and without candidate driver mutations, is common in the elderly. *Blood* **130**, 742–752 (2017).
12. Jaiswal, S. et al. Clonal hematopoiesis and risk of atherosclerotic cardiovascular disease. *N. Engl. J. Med.* **377**, 111–121 (2017).
13. Acuna-Hidalgo, R. et al. Ultra-sensitive sequencing identifies high prevalence of clonal hematopoiesis-associated mutations throughout adult life. *Am. J. Hum. Genet.* **101**, 50–64 (2017).
14. Laken, S. J. et al. Familial colorectal cancer in Ashkenazim due to a hypermutable tract in *APC*. *Nat. Genet.* **17**, 79–83 (1997).
15. Jones, A. V. et al. *JAK2* haplotype is a major risk factor for the development of myeloproliferative neoplasms. *Nat. Genet.* **41**, 446–449 (2009).
16. Kilpivaara, O. et al. A germline *JAK2* SNP is associated with predisposition to the development of *JAK2*(V617F)-positive myeloproliferative neoplasms. *Nat. Genet.* **41**, 455–459 (2009).
17. Olcaydu, D. et al. A common *JAK2* haplotype confers susceptibility to myeloproliferative neoplasms. *Nat. Genet.* **41**, 450–454 (2009).
18. Koren, A. et al. Genetic variation in human DNA replication timing. *Cell* **159**, 1015–1026 (2014).
19. Zhou, W. et al. Mosaic loss of chromosome Y is associated with common variation near *TCL1A*. *Nat. Genet.* **48**, 563–568 (2016).
20. Hinds, D. A. et al. Germ line variants predispose to both *JAK2* V617F clonal hematopoiesis and myeloproliferative neoplasms. *Blood* **128**, 1121–1128 (2016).
21. Wright, D. J. et al. Genetic variants associated with mosaic Y chromosome loss highlight cell cycle genes and overlap with cancer susceptibility. *Nat. Genet.* **49**, 674–679 (2017).
22. Sudlow, C. et al. UK biobank: an open access resource for identifying the causes of a wide range of complex diseases of middle and old age. *PLoS Med.* **12**, e1001779 (2015).
23. Loh, P.-R., Palamara, P. F. & Price, A. L. Fast and accurate long-range phasing in a UK Biobank cohort. *Nat. Genet.* **48**, 811–816 (2016).
24. Loh, P.-R. et al. Reference-based phasing using the Haplotype Reference Consortium panel. *Nat. Genet.* **48**, 1443–1448 (2016).
25. Machiela, M. J. et al. Mosaic chromosome 20q deletions are more frequent in the aging population. *Blood Advances* **1**, 380–385 (2017).
26. Fischbach, G. D. & Lord, C. The Simons Simplex Collection: a resource for identification of autism genetic risk factors. *Neuron* **68**, 192–195 (2010).
27. Werling, D. M. et al. An analytical framework for whole-genome sequence association studies and its implications for autism spectrum disorder. *Nat. Genet.* **50**, 727–736 (2018).
28. Beroukhim, R. et al. The landscape of somatic copy-number alteration across human cancers. *Nature* **463**, 899–905 (2010).
29. Davoli, T. et al. Cumulative haploinsufficiency and triplosensitivity drive aneuploidy patterns and shape the cancer genome. *Cell* **155**, 948–962 (2013).
30. Machiela, M. J. et al. Female chromosome X mosaicism is age-related and preferentially affects the inactivated X chromosome. *Nat. Commun.* **7**, 11843 (2016).
31. Sinclair, E. J., Potter, A. M., Watmore, A. E., Fitchett, M. & Ross, F. Trisomy 15 associated with loss of the Y chromosome in bone marrow: a possible new aging effect. *Cancer Genet. Cytogenet.* **105**, 20–23 (1998).
32. Landau, D. A. et al. Mutations driving CLL and their evolution in progression and relapse. *Nature* **526**, 525–530 (2015).
33. Puente, X. S. et al. Non-coding recurrent mutations in chronic lymphocytic leukaemia. *Nature* **526**, 519–524 (2015).
34. Sutherland, G. R., Baker, E. & Seshadri, R. S. Heritable fragile sites on human chromosomes. V. A new class of fragile site requiring BrdU for expression. *Am. J. Hum. Genet.* **32**, 542–548 (1980).
35. Hewett, D. R. et al. *FRA10B* structure reveals common elements in repeat expansion and chromosomal fragile site genesis. *Mol. Cell* **1**, 773–781 (1998).
36. Richards, R. I. & Sutherland, G. R. Dynamic mutations: a new class of mutations causing human disease. *Cell* **70**, 709–712 (1992).
37. Gurney, A. L., Carver-Moore, K., de Sauvage, F. J. & Moore, M. W. Thrombocytopenia in c-mpl-deficient mice. *Science* **265**, 1445–1447 (1994).
38. Tefferi, A. Novel mutations and their functional and clinical relevance in myeloproliferative neoplasms: *JAK2*, *MPL*, *TET2*, *ASXL1*, *CBL*, *IDH* and *IKZF1*. *Leukemia* **24**, 1128–1138 (2010).
39. Tukiainen, T. et al. Landscape of X chromosome inactivation across human tissues. *Nature* **550**, 244–248 (2017).
40. Loh, P.-R. et al. Contrasting genetic architectures of schizophrenia and other complex diseases using fast variance-components analysis. *Nat. Genet.* **47**, 1385–1392 (2015).
41. Oddsson, A. et al. The germline sequence variant rs2736100_C in *TERT* associates with myeloproliferative neoplasms. *Leukemia* **28**, 1371–1374 (2014).
42. Stacey, S. N. et al. A germline variant in the *TP53* polyadenylation signal confers cancer susceptibility. *Nat. Genet.* **43**, 1098–1103 (2011).
43. Rawstron, A. C. et al. Monoclonal B-cell lymphocytosis and chronic lymphocytic leukemia. *N. Engl. J. Med.* **359**, 575–583 (2008).
44. Landgren, O. et al. B-cell clones as early markers for chronic lymphocytic leukemia. *N. Engl. J. Med.* **360**, 659–667 (2009).
45. Landau, D. A. et al. Evolution and impact of subclonal mutations in chronic lymphocytic leukemia. *Cell* **152**, 714–726 (2013).
46. Ojha, J. et al. Monoclonal B-cell lymphocytosis is characterized by mutations in CLL putative driver genes and clonal heterogeneity many years before disease progression. *Leukemia* **28**, 2395–2398 (2014).
47. Berndt, S. I. et al. Meta-analysis of genome-wide association studies discovers multiple loci for chronic lymphocytic leukemia. *Nat. Commun.* **7**, 10933 (2016).
48. O'Keefe, C., McDevitt, M. A. & Maciejewski, J. P. Copy neutral loss of heterozygosity: a novel chromosomal lesion in myeloid malignancies. *Blood* **115**, 2731–2739 (2010).
49. Chase, A. et al. Profound parental bias associated with chromosome 14 acquired uniparental disomy indicates targeting of an imprinted locus. *Leukemia* **29**, 2069–2074 (2015).
50. Choate, K. A. et al. Mitotic recombination in patients with ichthyosis causes reversion of dominant mutations in *KRT10*. *Science* **330**, 94–97 (2010).

Acknowledgements We thank Y. Jakubek for assistance with follow-up on del(10q) events[8] and G. Bhatia, A. Gusev, M. Lipson, X. Liu, L. O'Connor, N. Patterson, and B. van de Geijn for discussions. This research was conducted using the UK Biobank Resource under Application #19808. A.L.P. was supported by NIH grants R01 HG006399, R01 GM105857, R01 MH101244, and R21 HG009513. P.-R.L. was supported by NIH fellowship F32 HG007805, a Burroughs Wellcome Fund Career Award at the Scientific Interfaces, and the Next Generation Fund at the Broad Institute of MIT and Harvard. G.G., R.E.H., and S.A.M. were supported by NIH grant R01 HG006855 and the the Stanley Center for Psychiatric Research. H.K.F. was supported by the Fannie and John Hertz Foundation. Y.A.R. was supported by NIH award T32 GM007753, a National Defense Science and Engineering Graduate Fellowship, and the Paul and Daisy Soros Foundation. S.F.B. and G.G. were supported by US Department of Defense Breast Cancer Research Breakthrough Awards W81XWH-16-1-0315 and W81XWH-16-1-0316 (project BC151244). S.F.B. was supported by the Elsa U. Pardee Foundation and NCI MSKCC Cancer Center Core Grant P30 CA008748. M.E.T. was supported, in part, by NIH grants UM1 HG008900 and R01 HD081256. Computational analyses were performed on the Orchestra High Performance Compute Cluster at Harvard Medical School, which is partially supported by grant NCRR 1S10RR028832-01, and on the Genetic Cluster Computer (http://www.geneticcluster.org) hosted by SURFsara and financially supported by the Netherlands Scientific Organization (NWO 480-05-003 PI: Posthuma) along with a supplement from the Dutch Brain Foundation and the VU University Amsterdam. This work was supported by a grant from the Simons Foundation (SFARI Awards #346042 and #385027, M.E.T.). We are grateful to all of the families at the participating Simons Simplex Collection (SSC) sites, as well as the principal investigators (A. Beaudet, R. Bernier, J. Constantino, E. Cook, E. Fombonne, D. Geschwind, R. Goin-Kochel, E. Hanson, D. Grice, A. Klin, D. Ledbetter, C. Lord, C. Martin, D. Martin, R. Maxim, J. Miles, O. Ousley, K. Pelphrey, B. Peterson, J. Piggot, C. Saulnier, M. State, W. Stone, J. Sutcliffe, C. Walsh, Z. Warren and E. Wijsman). We appreciate access to genetic and phenotypic data on SFARI Base.

Reviewer information *Nature* thanks S. Chanock, D. Conrad, I. Hall and the other anonymous reviewer(s) for their contribution to the peer review of this work.

Author contributions P.-R.L., G.G., S.F.B., S.A.M., and A.L.P. designed the study. P.-R.L. and G.G. analysed UK Biobank data. R.E.H. analysed SSC data. P.-R.L., G.G., H.K.F., and Y.A.R. developed statistical methods. P.F.P. assisted with IBD analyses. B.M.B. assisted with cancer phenotype curation. M.E.T. and S.A.M. supervised SSC analyses. All authors wrote the paper.

Competing interests The authors declare no competing interests.

Additional information

Extended data is available for this paper at https://doi.org/10.1038/s41586-018-0321-x.
Supplementary information is available for this paper at https://doi.org/10.1038/s41586-018-0321-x.
Reprints and permissions information is available at http://www.nature.com/reprints.
Correspondence and requests for materials should be addressed to P.-R.L. or G.G. or S.A.M. or A.L.P.

METHODS

No statistical methods were used to predetermine sample size. The experiments were not randomized and the investigators were not blinded to allocation during experiments and outcome assessment.

UK Biobank cohort and genotyping intensity data. The UK Biobank is a very large prospective study of individuals aged 40–70 years at assessment[22]. Participants attended assessment centres between 2006 and 2010, where they contributed blood samples for genotyping and blood analysis and answered questionnaires about medical history and environmental exposures. In the years since assessment, health outcome data for these individuals (for example, cancer diagnoses and deaths) have been accrued via UK national registries.

We analysed genetic data from the UK Biobank interim release (about 30% of the full UK Biobank) consisting of 152,729 samples typed on the Affymetrix UK BiLEVE and UK Biobank Axiom arrays with about 800,000 SNPs each and more than 95% overlap. We removed 480 individuals marked for exclusion from genomic analyses based on missingness and heterozygosity filters and one individual who had withdrawn consent, leaving 152,248 samples. We restricted the variant set to biallelic variants with missingness $\leq 10\%$ and we further excluded 111 variants found to have significantly different allele frequencies between the UK BiLEVE array and the UK Biobank array, leaving 725,664 variants on autosomes and the X chromosome. Finally, we additionally excluded 118,139 variants for which fewer than 10 samples (or for chrX, fewer than 5 female samples) were called as homozygous for the minor allele; we observed that genotype calls at these variants were susceptible to errors in which rare homozgyotes were called as heterozygotes. We phased the remaining 607,525 variants using Eagle2[24] with –Kpbwt = 40,000 and otherwise default parameters.

We transformed genotyping intensities to $\log_2$R ratio (LRR) and B-allele frequency (BAF) values[51] (which measure total and relative allelic intensities) after affine-normalization and GC wave-correction[52] in a manner similar to that described[1] (Supplementary Note 1). For each sample, we then computed s.d. (BAF) among heterozygous sites within each autosome, and we removed 320 samples with median s.d. (BAF) > 0.11 indicating low genotyping quality. Finally, we removed an additional 725 samples with evidence of possible contamination[8] (based on apparent short interstitial CNN-LOH events in regions of long-range linkage disequilibrium; Supplementary Note 1) and one sample without phenotype data, leaving 151,202 samples for analysis.

Detection of mCAs using long-range haplotype phase. Here we outline the key ideas of our approach to mCA detection; full details are provided in Supplementary Note 1. The core intuition is to harness long-range phase information to search for local imbalances between maternal and paternal allelic fractions in a cell population (Extended Data Fig. 1). The utility of haplotype phase for this purpose has previously been recognized[8,53,54], but previous approaches have needed to account for phase switch errors occurring roughly every megabase, a general challenge faced by haplotype-based analyses[55]. In the UK Biobank, we have phase information accurate at the scale of tens of megabases[23,24], enabling a new modelling approach and considerable gains in sensitivity for detection of large events at low cell fractions (Supplementary Note 5). (Because our method is phase-based, it has the limitation that it cannot detect events contained within regions of homozygosity. While this issue is minor in our study of large events, other approaches originally developed for detection of shorter constitutional or high-cell-fraction CNVs are not subject to this limitation[56,57].)

Our technique employs a three-state hidden Markov model (HMM) to capture mCA-induced deviations in allelic balance ($|\Delta\text{BAF}|$) at heterozygous sites. (By contrast, the hapLOH method[8,54] tabulates 'switch consistency' between consecutive heterozygous sites.) Our model has a single parameter Θ, which represents the expected absolute BAF deviation at germline hets within an mCA. In computationally phased genotyping intensity data, multiplying phase calls with (signed) BAF deviations produces contiguous regions within the mCA in which the expected phased BAF deviation is either $+\Theta$ or $-\Theta$ (with sign flips at phase switch errors); outside the mCA, no BAF deviation is expected. The three states of our HMM encode these three possibilities, and emissions from the states represent noisy BAF measurements. Transitions between the $+\Theta$ and $-\Theta$ states represent switch errors, while transitions between $\pm\,\Theta$ and the 0 state capture mCA boundaries.

Modelling observed phased BAF deviations using a parameterized HMM has the key benefit of naturally producing a likelihood ratio test statistic for determining whether a chromosome contains a mCA. Explicitly, for a given choice of Θ, we can compute the total probability of the observed BAF data under the assumption that mCA-induced BAF deviations have $E[|\Delta\text{BAF}|] = \Theta$, using standard HMM dynamic programming computations to integrate over uncertainty in phase switches and mCA boundaries. Taking the ratio of the maximum likelihood over all possible choices of Θ to the likelihood for $\Theta = 0$ (that is, no mCA) yields a test statistic. If the HMM perfectly represented the data, this test statistic could be compared to an asymptotic distribution. However, we know in practice that parameters within the HMM (for example, transition probabilities) are imperfectly estimated, so we instead calibrated our test statistic empirically: we estimated its null distribution by computing test statistics on data with randomized phase, and we used this empirical null to control FDR. Finally, for chromosomes passing the FDR threshold, we called mCA boundaries by sampling state paths from the HMM (using the maximum likelihood value of Θ).

The above detection procedure uses only BAF data and ignores LRR measurements by design (to be maximally robust to genotyping artefacts); however, after detecting events, we incorporated LRR data to call detected mCAs as loss, CNN-LOH, or gain. All mosaic chromosomal alterations cause BAF (measuring relative allelic intensity) to deviate from 0.5 at heterozygous sites, and losses and gains cause LRR (measuring total intensity) to deviate from 0, with deviations increasing with clonal cell fraction; accordingly, we observed that plotting detected events by LRR and BAF deviation produced three linear clusters (Fig. 2a), consistent with previous work[1,2,8]. We called copy number using chromosome-specific clusters to take advantage of the differing frequencies of event types on different chromosomes. Because the clusters converge as BAF deviation approaches zero, we left copy number uncalled for detected mCAs at low cell fraction (with <95% confident copy number), comprising 29% of all detected mCAs. We then estimated clonal cell fractions as described[1].

As a post-processing step to exclude possible constitutional duplications, we filtered events of length >10 Mb with LRR >0.35 or with LRR >0.2 and $|\Delta\text{BAF}|>0.16$, and we filtered events of length <10 Mb with LRR >0.2 or with LRR >0.1 and $|\Delta\text{BAF}|>0.1$. We chose these thresholds conservatively based on visual inspection of LRR and BAF distributions, in which likely constitutional duplications formed well-defined clusters (Supplementary Note 1). (Most constitutional duplications were already masked in a pre-processing step involving a separate HMM described in Supplementary Note 1.)

Enrichment of mCA types in blood lineages. We analysed 14 blood count indices (counts and percentages of lymphocytes, basophils, monocytes, neutrophils, red cells, and platelets, as well as distribution widths of red cells and platelets) from complete blood count data available for 97% of participants. We restricted the analysis to individuals of self-reported European ancestry (96% of the cohort), leaving 140,250 individuals; we then stratified by sex and quantile-normalized each blood index after regressing out age, age squared, and smoking status.

To identify classes of mCAs linked to different blood cell types, we first classified mCAs based on chromosomal location and copy number. For each autosome, we defined five disjoint categories of mCAs that comprised the majority of detected events: loss on p arm, loss on q arm, CNN-LOH on p arm, CNN-LOH on q arm, and gain. We subdivided loss and CNN-LOH events by arm but did not subdivide gain events because most gain events are whole-chromosome trisomies (Fig. 1). For chromosome X, we replaced the two loss categories with a single whole-chromosome loss category. Altogether, this classification resulted in 114 mCA types. We restricted our blood cell enrichment analyses to 78 mCA types with at least 10 occurrences, and we further excluded the chr17 gain category (because nearly all of these events arise from i(17q) isochromosomes already counted as 17p– events; Supplementary Note 2).

For each of the 77 remaining mCA types, we computed enrichment of mCAs among individuals with anomalous (top 1%) values of each normalized blood index using Fisher's exact test (two-sided; *P* values reported throughout this manuscript are from two-sided statistical tests unless explicitly stated otherwise). We reported significant enrichments passing an FDR threshold of 0.05 (Fig. 2f and Supplementary Table 6).

Chromosome-wide association tests for *cis* associations with mCAs. To identify inherited variants influencing nearby mCAs, we performed two types of association analysis. First, we searched for variants that increased the probability of developing nearby mCAs. For each variant, we performed a Fisher test for association between the variant and up to three variant-specific case-control phenotypes, defined by considering samples to be cases if they contained loss, CNN-LOH, or gain events containing the variant or within 4 Mb (to allow for uncertainty in event boundaries). We tested phenotypes with at least 25 cases; in total, 48 out of $69 = 23 \times 3$ possible event types had at least 25 carriers, and the rest were excluded from association analyses. We performed these tests on 51 million imputed variants with minor allele frequency (MAF) $> 2 \times 10^{-5}$ (imputed by UK Biobank using merged UK10K and 1000 Genomes Phase 3 reference panels[58]), excluding variants with non-European MAF greater than five times their European MAF, which tended to be poorly imputed. We analysed 120,664 individuals who remained after restricting to individuals of self-reported British or Irish ancestry, removing principal component outliers (>4 s.d.), and imposing a relatedness cutoff of 0.05 (using plink --rel-cutoff 0.05)[59]. (In our non-GWAS analyses, which focused on mosaic individuals, we did not apply any special handling of related individuals as the number of related pairs was very small: for example, only 11 third-degree or closer relationships among 4,889 individuals with autosomal mosaicism.)

We also ran a second form of association analysis searching for variants for which mCAs tended to shift allelic balance (analogous to allele-specific

expression). For a given class of mCAs, for each variant, we examined heterozygous mosaic individuals for which the mCA overlapped the variant, and we performed a binomial test to check whether the mCA was more likely to delete or duplicate one allele rather than the other. We restricted the binomial test to individuals in which the variant was confidently phased relative to the mCA (that is, no disagreement in five random resamples from the HMM used to call the mCA).

Given that the two association tests described above are independent, we applied a two-stage approach to identify robust genome-wide significant associations. We used a P value threshold of 10^{-8} for discovery in either test and then checked for nominal $P < 0.05$ significance in the other test (reasoning that variants that influenced mCAs would exhibit both types of association). At all loci with $P < 10^{-8}$ for either test, the most significant variant with $P < 10^{-8}$ in one test reached nominal significance in the other (Table 1). At identified loci, we further searched for secondary independent associations reaching $P < 10^{-6}$.

In our final analyses, we refined mCA phenotypes to slightly increase power to map associations. For the loci associated with 1p, 9p, and 15q CNN-LOH, we found that association strength improved by expanding case status to include all events reaching the telomere (because several detected telomeric events with uncertain copy number were probably actually CNN-LOH events associated with the same germline variants). For the association signal at *FRA10B*, we refined case status to only include terminal loss events extending from 10q25 to the telomere (because of the breakpoint specificity of this event). We verified that all association tests produced well-calibrated test statistics (Supplementary Note 3).

Identity-by-descent analysis at *MPL* and *FRA10B*. At loci for which we found evidence of multiple causal rare variants, we searched for long haplotypes shared identical-by-descent among mCA carriers to further explore the possibility of additional or recurrent causal variants. We called IBD tracts using GERMLINE with haplotype extension[60].

Simons Simplex Collection WGS data set. The Simons Simplex Collection (SSC) is a repository of genetic samples from autism simplex families collected by the Simons Foundation Autism Research Initiative (SFARI)[26]. We analysed 2,079 whole-genome sequences from the first phase of SSC sequencing (median coverage 37.8×)[27] to examine whether mCAs we detected contributed to genetic risk of autism. (The main data set consisted of 2,076 individuals in 519 quartets; we additionally analysed three individuals that did not belong to a complete quartet but were of interest based on high read counts at *FRA10B*.)

Detection and calling of 70-kb deletion at 15q26.3. We discovered the inherited 70-kb deletion associated with 15q CNN-LOH and loss by mapping the 15q26.3 association signal (specifically, the rs182643535 tag SNP) in WGS data (Fig. 4c and Extended Data Fig. 6). We then called this deletion in the UK Biobank SNP-array data using genotyping intensities at 24 probes in the deleted region (Extended Data Fig. 7).

Detection and imputation of VNTRs at *FRA10B*. For all WGS samples with 10 or more reads at the *FRA10B* locus, we attempted to perform local assembly of the reads and identify a primary VNTR motif in the assembly. We identified 12 distinct primary motifs carried by 26 individuals in 14 families (Extended Data Fig. 5a, b and Supplementary Note 8). Owing to read dropout in many samples, it is possible that these VNTR motifs may be found in additional samples, and that other VNTR motifs may not have been detected. We imputed the VNTR sequences into UK Biobank using Minimac3[61]. Full details are provided in Supplementary Note 8.

GWAS and heritability estimation for *trans* drivers of clonality. We tested variants with MAF > 1% for *trans* associations with six classes of mCAs (any event, any loss, any CNN-LOH, any gain, any autosomal event, any autosomal loss) on 120,664 unrelated individuals with European ancestry (described above) using BOLT-LMM[62], including 10 principal components, age, and genotyping array as covariates. We also tested association with female X loss using an expanded set of 3,462 likely X loss calls at an FDR of 0.1, restricting this analysis to 66,685 female individuals. In our targeted analysis of 86 variants implicated in previous GWAS, we applied a Bonferroni significance threshold of 8.3×10^{-5} based on 86 variants and 7 phenotypes. We estimated SNP heritability of X loss using BOLT-REML[40], transforming estimates to the liability scale[63].

Analysis of X chromosome inactivation in GEUVADIS RNA sequencing data. To test for possible mediation of preferential X haplotype loss by biased X chromosome inactivation (XCI), we examined GEUVADIS RNA sequencing (RNA-seq) data[64] for evidence of biased XCI near the primary biased loss association at Xp11.1. We identified three coding SNPs in *FAAH2* within the pericentromeric linkage disequilibrium block containing the association signal. We analysed RNA-seq data for 61 European-ancestry individuals who were heterozygous for at least one SNP (60 of 61 were heterozygous for all three SNPs, and the remaining individual was heterozygous at two of the SNPs). We used GATK ASEReadCounter[65] to identify allele-specific expression from RNA-seq BAM files. Most individuals displayed strong consistent allele-specific expression across the three SNPs, as expected for XCI in clonal lymphoblastoid cell lines[39]; however, we observed no evidence of systematically biased XCI in favour of one allele or the other (Supplementary Table 10).

UK Biobank cancer phenotypes. We analysed UK cancer registry data provided by UK Biobank for 23,901 individuals with one or more prevalent or incident cancer diagnoses. Cancer registry data included date of diagnosis and ICD-O-3 histology and behaviour codes, which we used to identify individuals with diagnoses of CLL, MPN, or any blood cancer[66,67]. Because our focus was on prognostic power of mCAs for predicting diagnoses of incident cancers more than one year after DNA collection, we excluded all individuals with cancers reported prior to this time (either from cancer registry data or self-report of prevalent cancers). We also restricted our attention to the first diagnosis of cancer in each individual, and we censored diagnoses after 30 September 2014, as suggested by UK Biobank (resulting in a median follow-up time of 5.7 years, s.d. 0.8 years, range 4–9 years). Finally, we restricted analyses to individuals with self-reported European ancestry. These exclusions reduced the total counts of incident cases to 78 (CLL), 42 (MPN), and 441 (any blood cancer), which we analysed with 119,330 controls. In our primary analyses, we further eliminated individuals with any evidence of potential undiagnosed blood cancer based on anomalous blood counts (lymphocyte count outside the normal range of $1–3.5 \times 10^9$/l, red cell count $>6.1 \times 10^{12}$/l for males or $>5.4 \times 10^{12}$/l for females, platelet count $>450 \times 10^9$/l, red cell distribution width >15%), leaving incident case counts of 36 (CLL), 23 (MPN), and 327 (any blood cancer).

Estimation of cancer risk conferred by mCAs. To identify classes of mCAs associated with incident cancer diagnoses, we classified mCAs based on chromosomal location and copy number into the 114 classes described above. We then restricted our attention to the 45 classes with at least 30 carriers (to reduce our multiple hypothesis burden, given that we would be underpowered to detect associations with the rarer events). For each mCA class, we considered a sample to be a case if it contained only the mCA or if the mCA had the highest cell fraction among all mCAs detected in the sample (that is, we did not count carriers of subclonal events as cases). We computed odds ratios and P values for association between mCA classes and incident cancers using Cochran–Mantel–Haenszel (CMH) tests to stratify by sex and by age (in six 5-year bins). We used the CMH test to compute odds ratios (for incident cancer any time during follow-up) rather than using a Cox proportional hazards model to compute hazard ratios because both the mCA phenotypes and the incident cancer phenotypes were rare, violating normal approximations underlying regression. We reported significant associations passing an FDR threshold of 0.05 (Fig. 5a and Supplementary Table 12).

Prediction of incident CLL. We considered four nested logistic models for prediction of incident CLL. In the first model, a baseline, we included only age and sex as explanatory variables. In the second model, we added CLL genetic risk (computed using 14 high-confidence GWAS hits that had both been previously published[47] and reached $P < 5 \times 10^{-8}$). In the third model, we added log lymphocyte count. In the full model, we added explanatory variables for 13q and +12 events.

We assessed the accuracy of each model on two benchmark sets of samples. We restricted our primary analyses to individuals with normal lymphocyte counts ($1–3.5 \times 10^9$/l) at assessment (that is, exhibiting at most slight clonality); in auxiliary analyses, we removed this restriction (and expanded the full prediction model to include 11q–, +12, 13q–, 13q CNN-LOH, 14q–, 22q–, and the total number of other autosomal events). We performed tenfold stratified cross-validation to compare model performance. We assessed prediction accuracy by merging results from all cross-validation folds and computing area under the receiver operating characteristic curve (AUC) (Fig. 5b), and we also measured precision-recall performance (Extended Data Fig. 9). (We caution that while AUC is commonly used to assess discriminative power, AUC does not have a direct clinical interpretation[68].)

Estimation of mortality risk conferred by mCAs. We analysed UK death registry data provided by UK Biobank for 4,619 individuals reported to have died since assessment. We censored deaths after 31 December 2015, as suggested by UK Biobank, leaving 4,518 reported deaths over a median follow-up time of 6.9 years (range 5–10 years). We examined the relationship between mCAs and mortality, aiming to extend previous observations that mosaic point mutations increase mortality risk[3,4,11]. For this analysis, we were insufficiently powered to stratify mCAs by chromosome owing to the weaker effects of mCAs on mortality risk and the relatively small number of deaths reported during follow-up. We therefore stratified mCAs only by copy number and computed the hazard ratio conferred by each event class using a Cox proportional hazards model. We restricted these analyses to individuals with self-reported European ancestry, and we adjusted for age and sex as well as smoking status, which was previously associated with clonal haematopoiesis[3,11,69] and associates with mosaicism in the UK Biobank ($P = 0.00017$). We did not exclude individuals based on blood counts in these analyses (or in our time-to-malignancy versus clonal fraction analyses), hence the larger sample sizes in Fig. 5c, d than in Fig. 5a, b.

Code availability. Code used to perform the analyses in this study is available from the corresponding authors upon request.

Data availability. Mosaic event calls are available in the Supplementary Data. Access to the UK Biobank Resource is available via application (http://www.ukbiobank.ac.uk/). Approved researchers can obtain the SSC population data set described in this study by applying at https://base.sfari.org.

51. Peiffer, D. A. et al. High-resolution genomic profiling of chromosomal aberrations using Infinium whole-genome genotyping. *Genome Res.* **16**, 1136–1148 (2006).
52. Diskin, S. J. et al. Adjustment of genomic waves in signal intensities from whole-genome SNP genotyping platforms. *Nucleic Acids Res.* **36**, e126 (2008).
53. Nik-Zainal, S. et al. The life history of 21 breast cancers. *Cell* **149**, 994–1007 (2012).
54. Vattathil, S. & Scheet, P. Haplotype-based profiling of subtle allelic imbalance with SNP arrays. *Genome Res.* **23**, 152–158 (2013).
55. Genovese, G., Leibon, G., Pollak, M. R. & Rockmore, D. N. Improved IBD detection using incomplete haplotype information. *BMC Genet.* **11**, 58 (2010).
56. Olshen, A. B., Venkatraman, E. S., Lucito, R. & Wigler, M. Circular binary segmentation for the analysis of array-based DNA copy number data. *Biostatistics* **5**, 557–572 (2004).
57. Pique-Regi, R., Cáceres, A. & González, J. R. R-Gada: a fast and flexible pipeline for copy number analysis in association studies. *BMC Bioinformatics* **11**, 380 (2010).
58. Huang, J. et al. Improved imputation of low-frequency and rare variants using the UK10K haplotype reference panel. *Nat. Commun.* **6**, 8111 (2015).
59. Chang, C. C. et al. Second-generation PLINK: rising to the challenge of larger and richer datasets. *Gigascience* **4**, 7 (2015).
60. Gusev, A. et al. Whole population, genome-wide mapping of hidden relatedness. *Genome Res.* **19**, 318–326 (2009).
61. Das, S. et al. Next-generation genotype imputation service and methods. *Nat. Genet.* **48**, 1284–1287 (2016).
62. Loh, P.-R. et al. Efficient Bayesian mixed-model analysis increases association power in large cohorts. *Nat. Genet.* **47**, 284–290 (2015).
63. Lee, S. H., Wray, N. R., Goddard, M. E. & Visscher, P. M. Estimating missing heritability for disease from genome-wide association studies. *Am. J. Hum. Genet.* **88**, 294–305 (2011).
64. Lappalainen, T. et al. Transcriptome and genome sequencing uncovers functional variation in humans. *Nature* **501**, 506–511 (2013).
65. Castel, S. E., Levy-Moonshine, A., Mohammadi, P., Banks, E. & Lappalainen, T. Tools and best practices for data processing in allelic expression analysis. *Genome Biol.* **16**, 195 (2015).
66. Turner, J. J. et al. InterLymph hierarchical classification of lymphoid neoplasms for epidemiologic research based on the WHO classification (2008): update and future directions. *Blood* **116**, e90–e98 (2010).
67. Arber, D. A. et al. The 2016 revision to the World Health Organization classification of myeloid neoplasms and acute leukemia. *Blood* **127**, 2391–2405 (2016).
68. Chatterjee, N., Shi, J. & García-Closas, M. Developing and evaluating polygenic risk prediction models for stratified disease prevention. *Nat. Rev. Genet.* **17**, 392–406 (2016).
69. Dumanski, J. P. et al. Mutagenesis. Smoking is associated with mosaic loss of chromosome Y. *Science* **347**, 81–83 (2015).

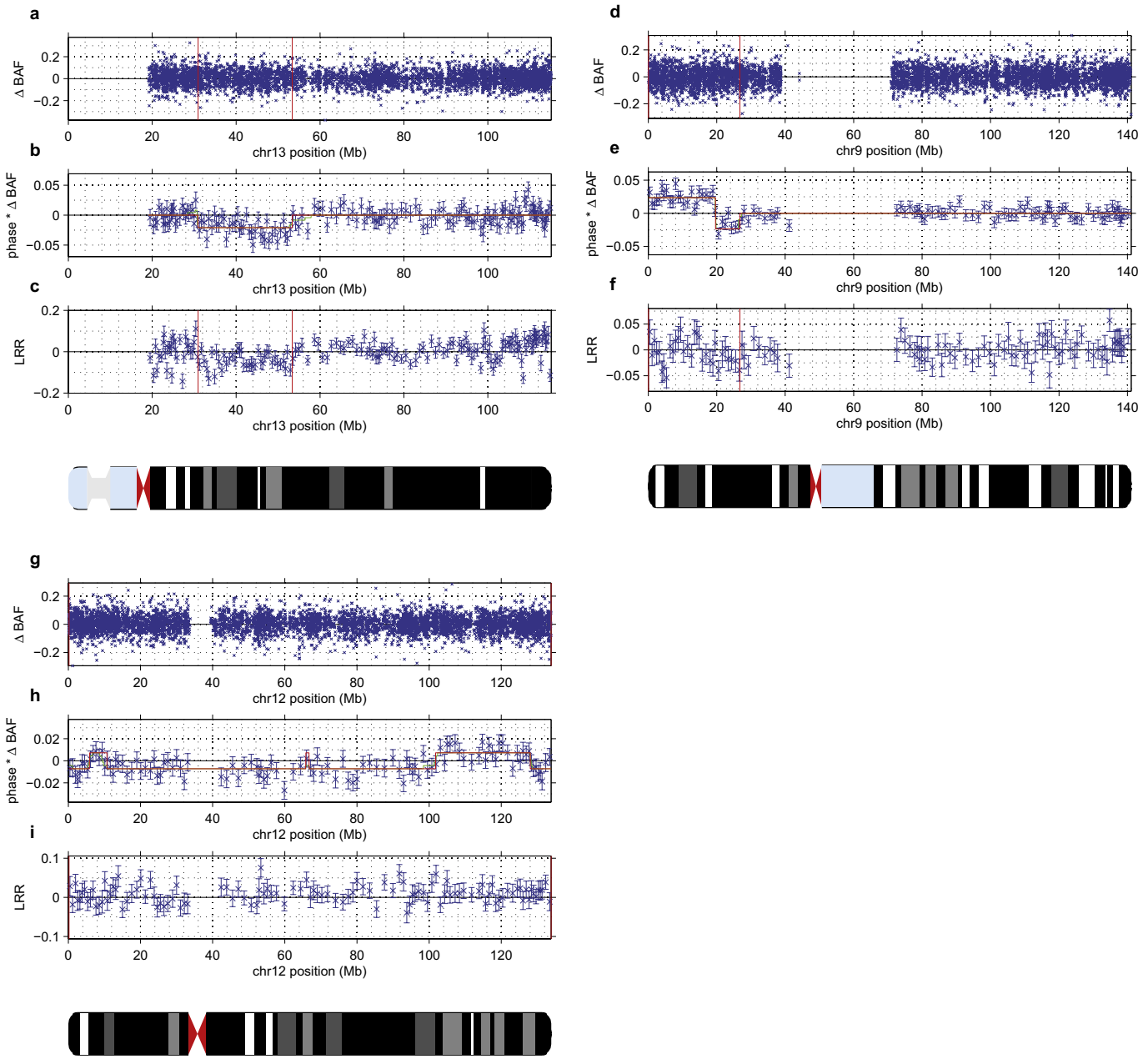

Extended Data Fig. 1 | Examples of mosaic events called using phased genotyping intensities. **a**–**c**, UK Biobank mCA sample 2791 has a mosaic deletion of chr13 from approximately 31–53 Mb that cannot be confidently called from unphased BAF and LRR data (**a**, **c**). However, the existence of an event is evident in the phased BAF data (**b**), and the regional decrease in LRR indicates that this event is a deletion. In **b**, mean phased BAF is plotted for SNPs aggregated into bins spanning $n = 25$ heterozygous sites; the same bins are used for **c**. Error bars, s.e.m. **d**–**f**, Sample 1645 has a mosaic CNN-LOH on chr9p from the 9p telomere to about 26 Mb that cannot be confidently called from unphased BAF data (**d**) but is evident in phased BAF data (**e**). A phase switch error causes a sign flip in phased BAF at approximately 20 Mb. The lack of a shift in LRR in the region (**f**) indicates that this event is a CNN-LOH. In **e**, mean phased BAF is plotted for SNPs aggregated into bins spanning $n = 50$ heterozygous sites; the same bins are used for **f**. Error bars, s.e.m. **g**–**i**, Sample 2464 has a full-chromosome mosaic event on chr12 that cannot be confidently called from unphased BAF and LRR data (**g**, **i**) but is evident in phased BAF data (**h**). Several phase switch errors cause sign flips in phased BAF across chr12. The slight positive shift in mean LRR (**i**) indicates that this event is most likely to be a mosaic gain of chr12. In **h**, mean phased BAF is plotted for SNPs aggregated into bins spanning $n = 50$ heterozygous sites; the same bins are used for **i**. Error bars, s.e.m.

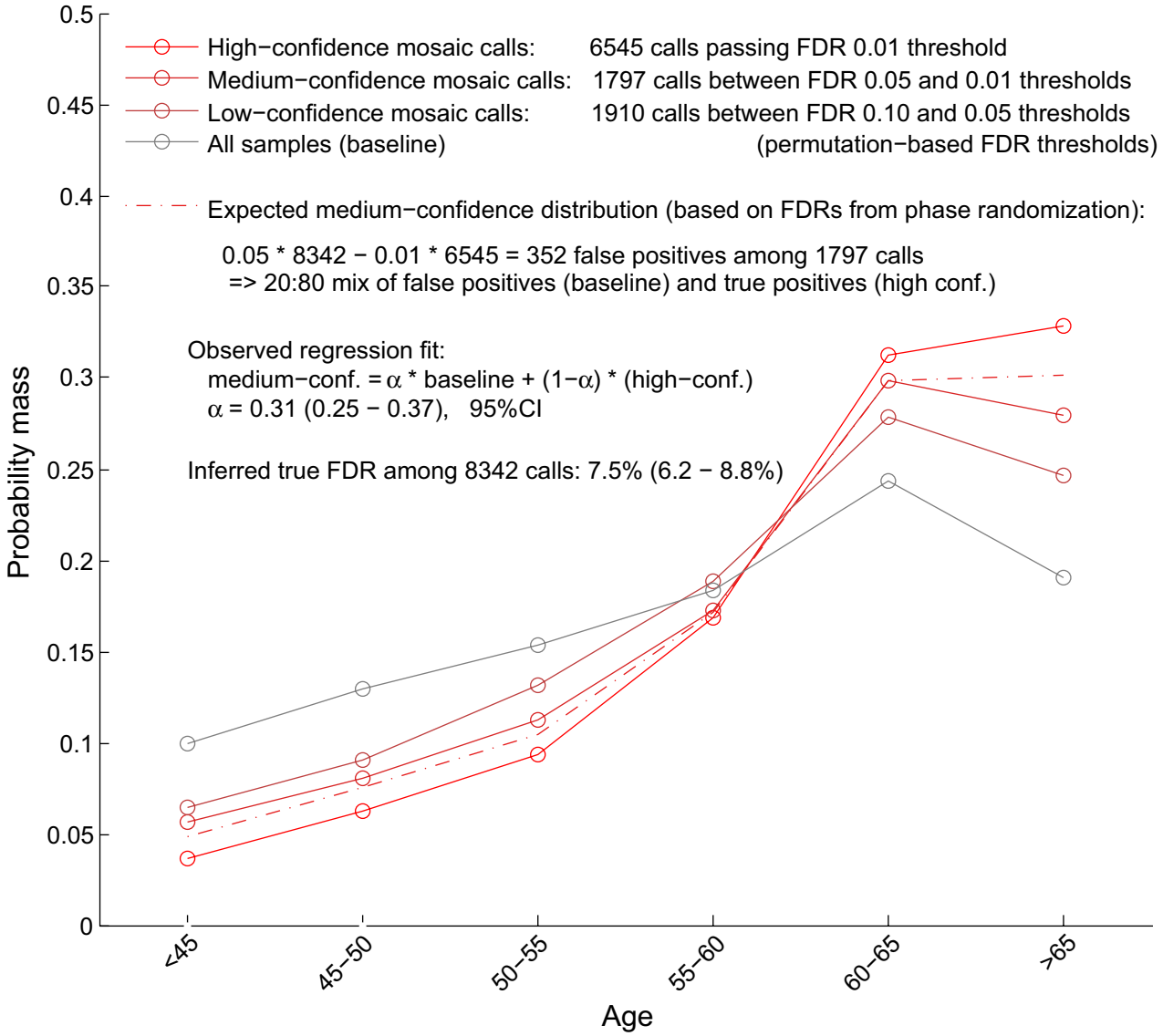

Extended Data Fig. 2 | Estimation of true FDR using age distributions of individuals with mCA calls. We generated age distributions for (i) 'high-confidence' detected events passing a permutation-based FDR threshold of 0.01 (bright red); (ii) 'medium-confidence' events below the FDR threshold of 0.01 but passing an FDR threshold of 0.05 (darker red); and (iii) 'low-confidence' events below the FDR threshold of 0.05 but passing an FDR threshold of 0.10 (darkest red; not analysed but plotted for context). We compared these distributions to the overall age distribution of UK Biobank participants (grey). On the basis of the numbers of events in each category, approximately 20% of medium-confidence detected events are expected to be false positives. To estimate our true FDR, we regressed the medium-confidence age distribution on the high-confidence and overall age distributions, reasoning that the medium-confidence age distribution should be a mixture of correctly called events with age distribution similar to that of the high-confidence events, and spurious calls with age distribution similar to the overall cohort. We observed a regression weight of 0.31 for the component corresponding to spurious calls, in good agreement with expectation, and implying a true FDR of 7.5% (6.2–8.8%, 95% CI based on regression fit on $n = 6$ age bins).

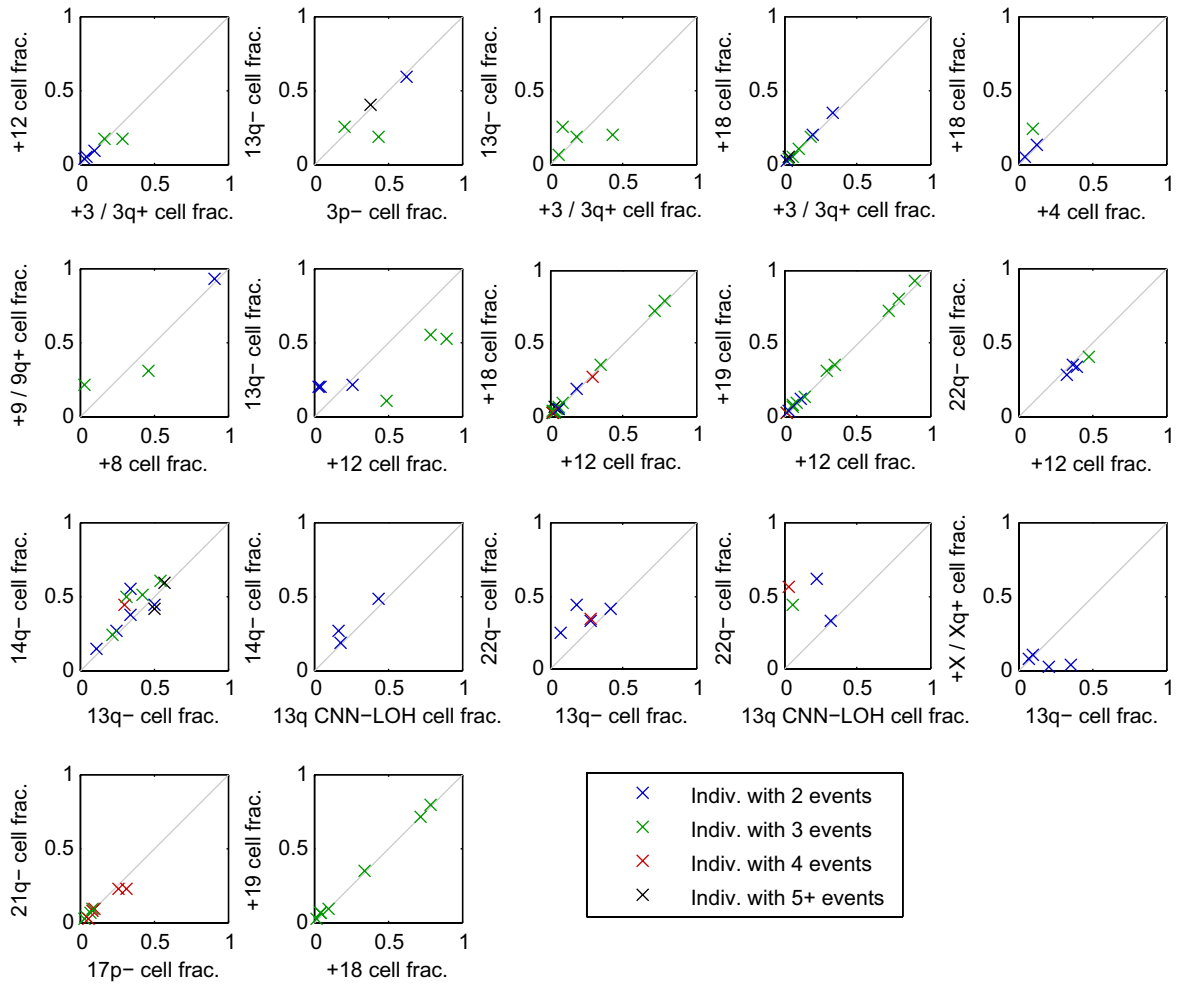

Extended Data Fig. 3 | Clonal cell fractions of co-occurring events generally suggest co-existence within the same cell population. For each pair of significantly co-occurring events (Fig. 2b), we compared the clonal fractions of the two events within each individual that carried both events. Each point in the plots corresponds to an individual carrying the pair of events under consideration; individuals are colour-coded by the total number of events they carry. For nearly all pairs of events, the clonal fractions of the two events were very similar in most individuals carrying both events, suggesting that the events occurred in the same clonal cell population. A few exceptions do seem to exist; for example, 22q− versus 13q CNN-LOH cell fraction; here, the cell fractions suggest that 13q CNN-LOH events may be present in a subclone. This observation is consistent with acquired uniparental disomy of 13q providing a second hit within a del(13q14) clonal expansion, as we see in Extended Data Fig. 8. (We did not include del(13q14) vs. 13q CNN-LOH in this plot because inference of clonal fractions is complex for these overlapping events; see Extended Data Fig. 8.)

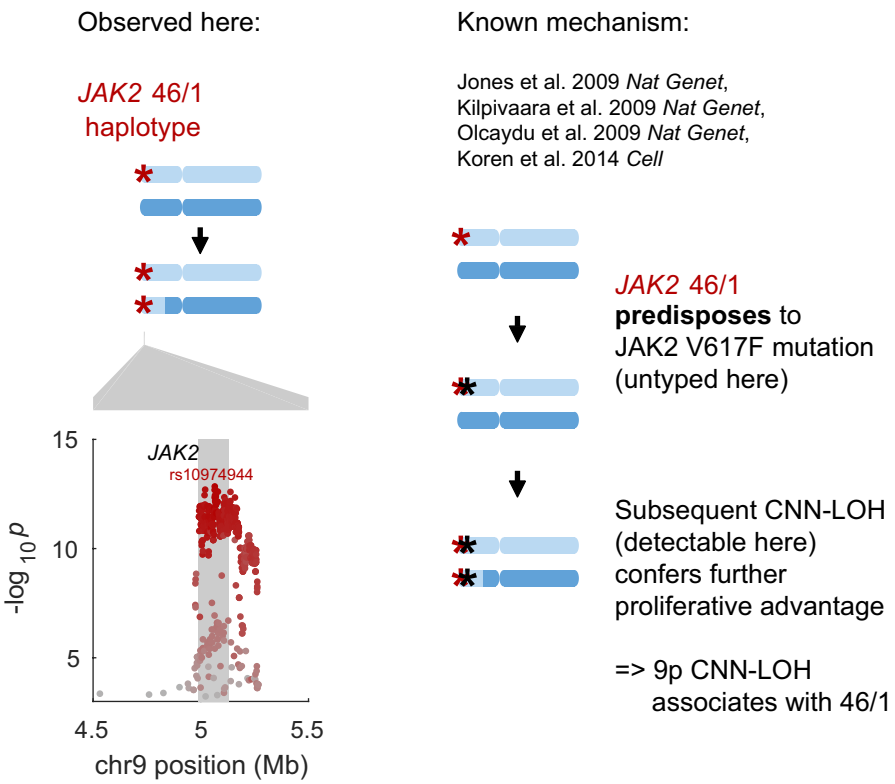

Extended Data Fig. 4 | Replication of previous association between *JAK2* 46/1 haplotype and 9p CNN-LOH in *cis* due to clonal selection. The common *JAK2* 46/1 haplotype has previously been shown to confer risk of somatic *JAK2* V617F mutation such that subsequent 9p CNN-LOH produces a strong proliferative advantage[15–18,20] (right). In our analysis, CNN-LOH on 9p is strongly associated with *JAK2* 46/1 ($P = 1.6 \times 10^{-13}$, OR = 2.7 (2.1–3.5); Fisher's exact test on $n = 120{,}664$ individuals) with the risk haplotype predominantly duplicated by CNN-LOH in hets (52 of $n = 61$ heterozygous cases; binomial $P = 1.8 \times 10^{-8}$). Left, the genomic modification is illustrated in the top panel and association signals are plotted in the bottom. The lead associated variant is labelled, and variants are coloured according to linkage disequilibrium with the lead variant (scaled for readability).

a Variable Number Tandem Repeats (VNTRs) at *FRA10B* identified in WGS data

```
VNTR-43-e     GATATAATATAT CGTATACAA TATATACGT ATATAT TATATAC
E13           GATATAATATAT CATATGTAA TAGATAT-G ATGTAT TACATAT
E11           GATATAATATAT CATATGTAA TAGATATGT ATATAT TATATAT
E12           GATATAATATAT CATATGTAA TAGATATGT ATATAT TACATAT
E8            GATATAATATAT ATTATATAA TATATATGT ATATAT TATATAT
VNTR-43-a     GATATAATATAT CGTATATAT TATATACGG ATACAT TATATAT
HG19-REF      GATATAATATAT ---ACATAT TATATATGT ATATAT TATATAT
VNTR-42-c     GATATAATATAT CATACATAT TATATAT-G ATATAT TATCTAT
VNTR-42-b     GATATAATATAT CATACATAT TATCTAT-G ATATAT TATATAT
VNTR-42-d     GATATAATATAT CATACATAT TATGTAT-G ATATAT TATATAT
VNTR-42-e     GATATCATATAT CATACATAT TATATAT-G ATATAT TATATAT
VNTR-39-a     GATATAATATAT C---CATAT TATATAT-G ATATAT TATATAT
VNTR-43-b     GATATAATATAT CATACATAT TATATATGG ATATAT TATATAT
VNTR-42-a     GATATAATATAT CATACATAT TATATAT-G ATATAT TATATAT
VNTR-38-a     GATATAATATAT C----ATAT TATATAC-G ATATAT GATATAT
E10           GATATAATATAT CATATATAA TATATATGT ATATAT TATATAT
VNTR-43-d     GATATAATATAT CATATATAA TATATATGG ATATAT TATATAT
E17           GATATAATATAT CATATATAA TATATAT-G ATATAT TATATAT
VNTR-43-c     GATATAATATAT CATATATAT TATATACGG ATATAT TATATAT
E19           GATATAATATAT CATATATAT TATATAT-G ATATAT TATATAT
              ***** ******       *  **  **    **  **  *  **
```

b Identity-by-descent graph at *FRA10B* for UK Biobank del(10q) individuals colored according to imputed VNTRs

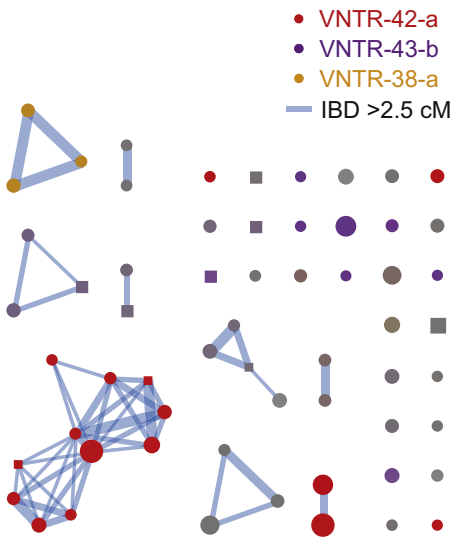

c IBD graph at *MPL* for UK Biobank 1p mosaic individuals

Edges = IBD>2.5cM (edge weights increase with IBD length)
Red nodes = carriers of rare MPL nonsense mutation (rs369156948)
Green nodes = carriers of long rare haplotype (tag: rs144279563)
Blue nodes = carriers of long rare haplotype (tag: rs182971382)

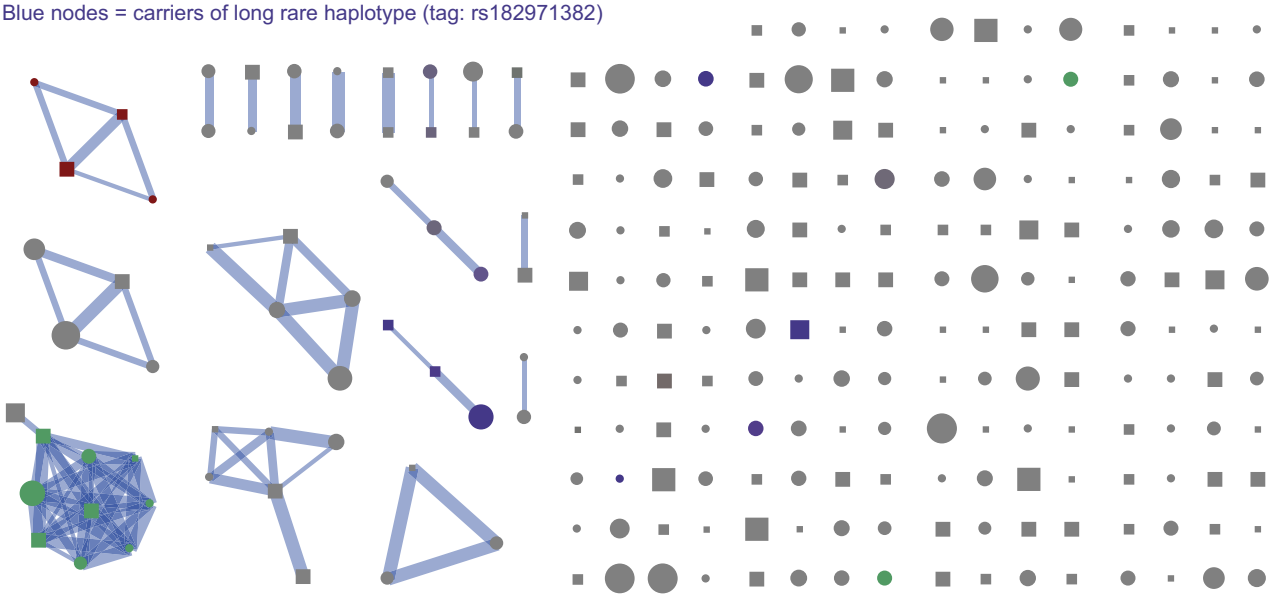

Extended Data Fig. 5 | Evidence of multiple causal variants for 10q25.2 breakage and 1p CNN-LOH associations. a, Multiple expanded repeats at *FRA10B* drive breakage at 10q25.2. We identified 12 distinct primary repeat motifs at *FRA10B* in 26 whole-genome-sequenced individuals from 14 families (labelled VNTR-*N*-x, where *N* denotes length in base pairs); carriers of these repeats exhibit varying degrees of *FRA10B* repeat expansion (Supplementary Note 8). The repeat motifs are AT-rich and are similar to *FRA10B* repeats previously reported[35]. The alignment provided here includes the repeat motifs that were most frequently observed in *FRA10B* expanded alleles[35] (E8, E13, E17, and E19) along with a few other closely related expanded repeat motifs (E10, E11, and E12). **b**, Carriers of the 10q terminal deletion in the UK Biobank share long haplotypes at 10q25.2 identical-by-descent. Square nodes in the IBD graph correspond to males and circles to females. Node size is proportional to cell fraction and edge weight increases with IBD length. Coloured nodes indicate imputed carriers of variable number tandem repeats (VNTRs) at *FRA10B* (Supplementary Table 7); colour intensity scales with imputed dosage. **c**, Identity-by-descent graph at *MPL* locus (chr1:43.8 Mb) on individuals with mCAs on chr1 extending to the p telomere. Colored nodes indicate imputed carriers of SNPs independently associated with mosaic 1p CNN-LOH (Fig. 4a).

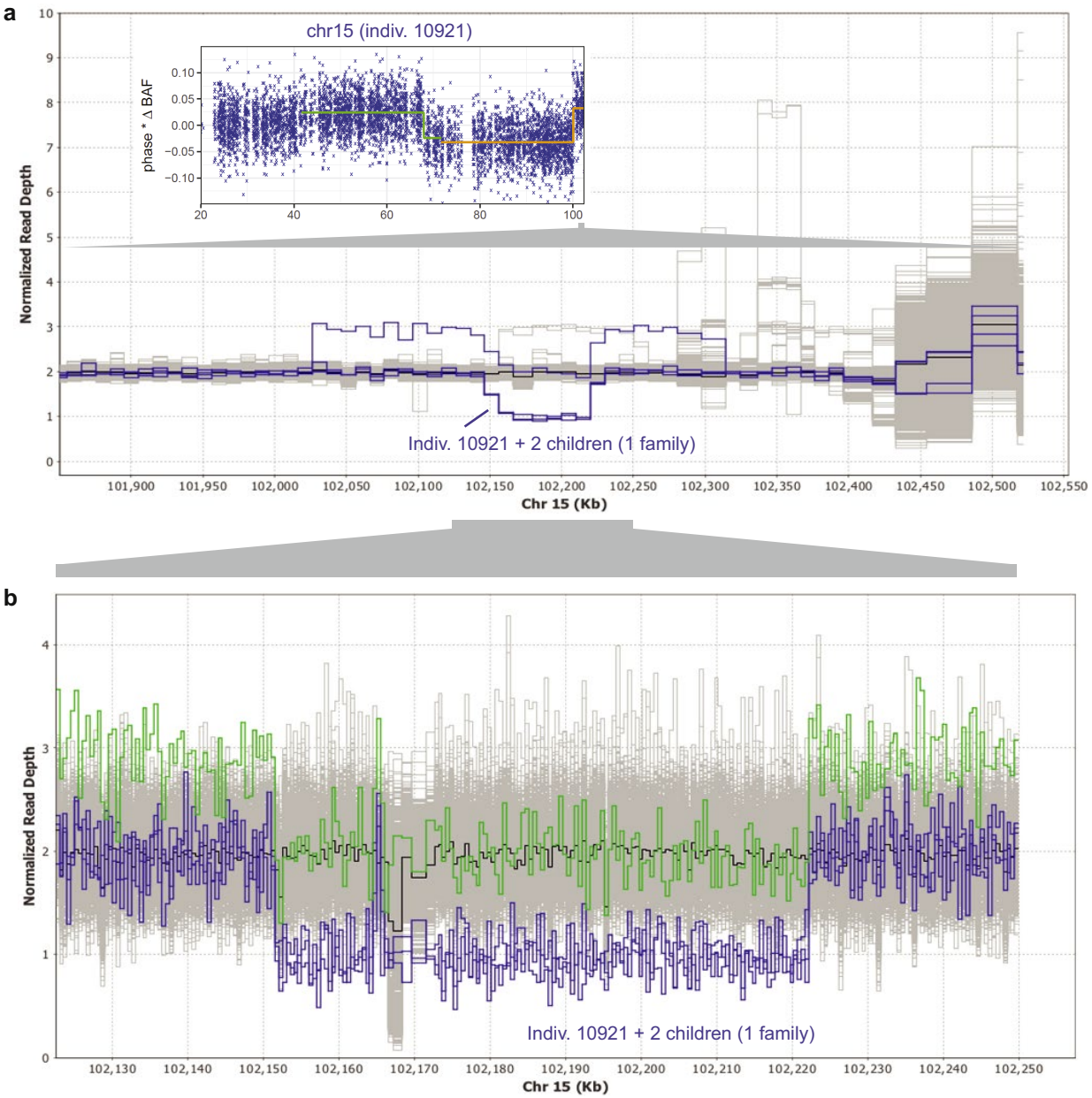

Extended Data Fig. 6 | Germline CNVs at 15q26.3. a, Read depth profile plot of WGS samples in the terminal 700 kb of chr15q. Three individuals in one family carry an approximately 70-kb deletion at 15q26.3, and a fourth carries the same deletion along with an approximately 290-kb duplication (probably on the same haplotype, based on population frequencies of these events; see Extended Data Fig. 7). These four individuals (highlighted in blue) segregate with the rs182643535:T allele in the WGS cohort. Inset: the parental carrier in the family, individual 10921, has detectable mosaicism in two distinct 15q CNN-LOH subclones (one starting at 41.64 Mb with 4.6% cell fraction, the other starting at 71.64 Mb with an additional 2.0% cell fraction). **b**, Expanded read depth profile plot, with deletion-only individuals highlighted in blue and the del + dup individual highlighted in green. Breakpoint analysis indicates that the deletion spans chr15:102151467–102222161 and contains a 1,139-bp mid-segment (chr15:102164897–102166035) that is retained in inverted orientation. The duplication spans chr15:102026997–102314016.

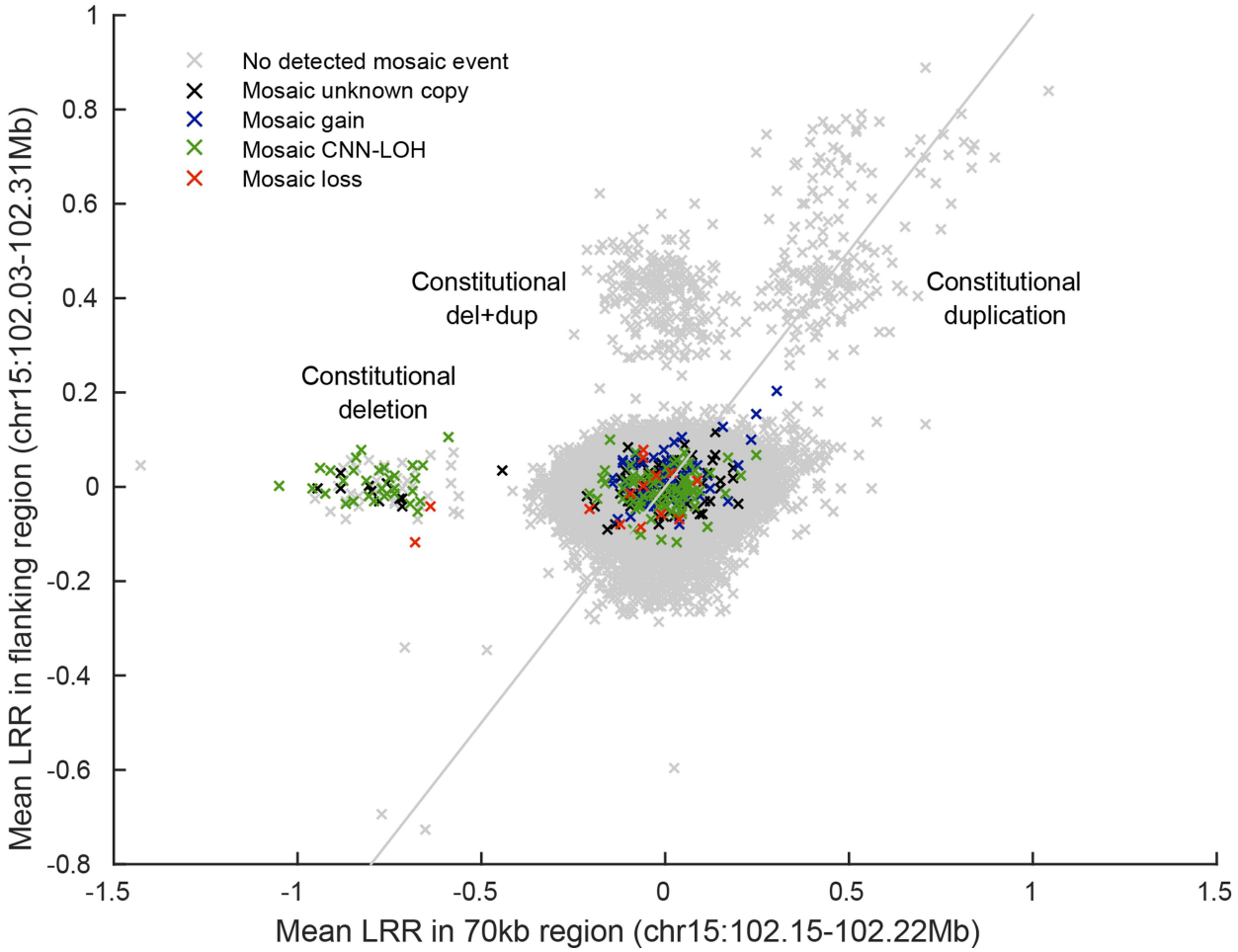

Extended Data Fig. 7 | Mosaic chromosomal alterations and germline CNVs at 15q26.3. Using identified breakpoints of the germline 70-kb deletion and 290-kb duplication (Extended Data Fig. 6), we computed mean genotyping intensity (LRR) in UK Biobank samples within the 70-kb deletion region (24 probes) and within the flanking 220-kb region (97 probes). Individuals are plotted by flanking 220-kb mean LRR versus 70-kb mean LRR and coloured according to mosaic status for somatic 15q mCAs. UK Biobank samples carrying the 70-kb deletion, 290-kb duplication, and both (del+dup) are all easily identifiable in distinct clusters. The plot also appears to contain clusters with higher copy number. Of the three CNV-carrying alleles, the simple 70-kb deletion is the only one that predisposes to mCAs. Most mosaic events containing the 70-kb deletion are CNN-LOH events that make cells homozygous for the 70-kb deletion; two individuals have somatic loss of the homologous (normal) chromosome, making cells hemizygous for the 70-kb deletion.

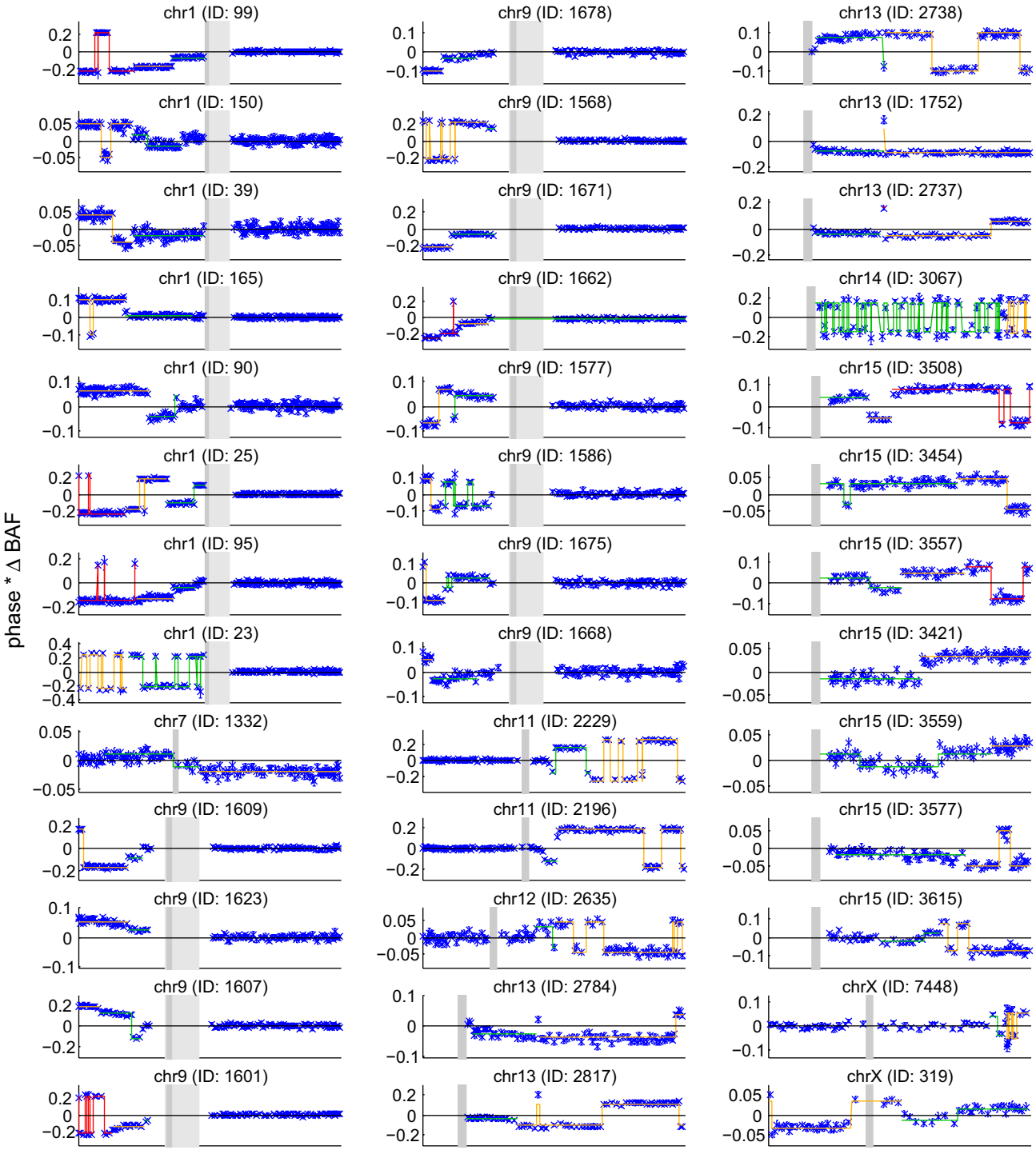

Extended Data Fig. 8 | Phased BAF plots of chromosomes with multiple CNN-LOH subclones. All of the plots exhibit step functions of increasing |ΔBAF| towards a telomere, which is the hallmark of multiple clonal cell populations containing distinct CNN-LOH events that affect different spans of a chromosomal arm (all extending to the telomere). Distinct |ΔBAF| values (called using an HMM) are indicated with different colours. Flips in the sign of phased BAF usually correspond to phase switch errors. Two samples exhibit high switch error rates: 14q individual 3067 (explained by non-European ancestry), and 1p individual 23 (explained by very high |ΔBAF|; extreme shifts in genotyping intensities result in poor genotyping quality). All five individuals with multiple CNN-LOH events on chr13q appear to contain switch errors over 13q14, but these switches are actually explained by overlapping 13q14 deletions; see Supplementary Note 1 for detailed discussion.

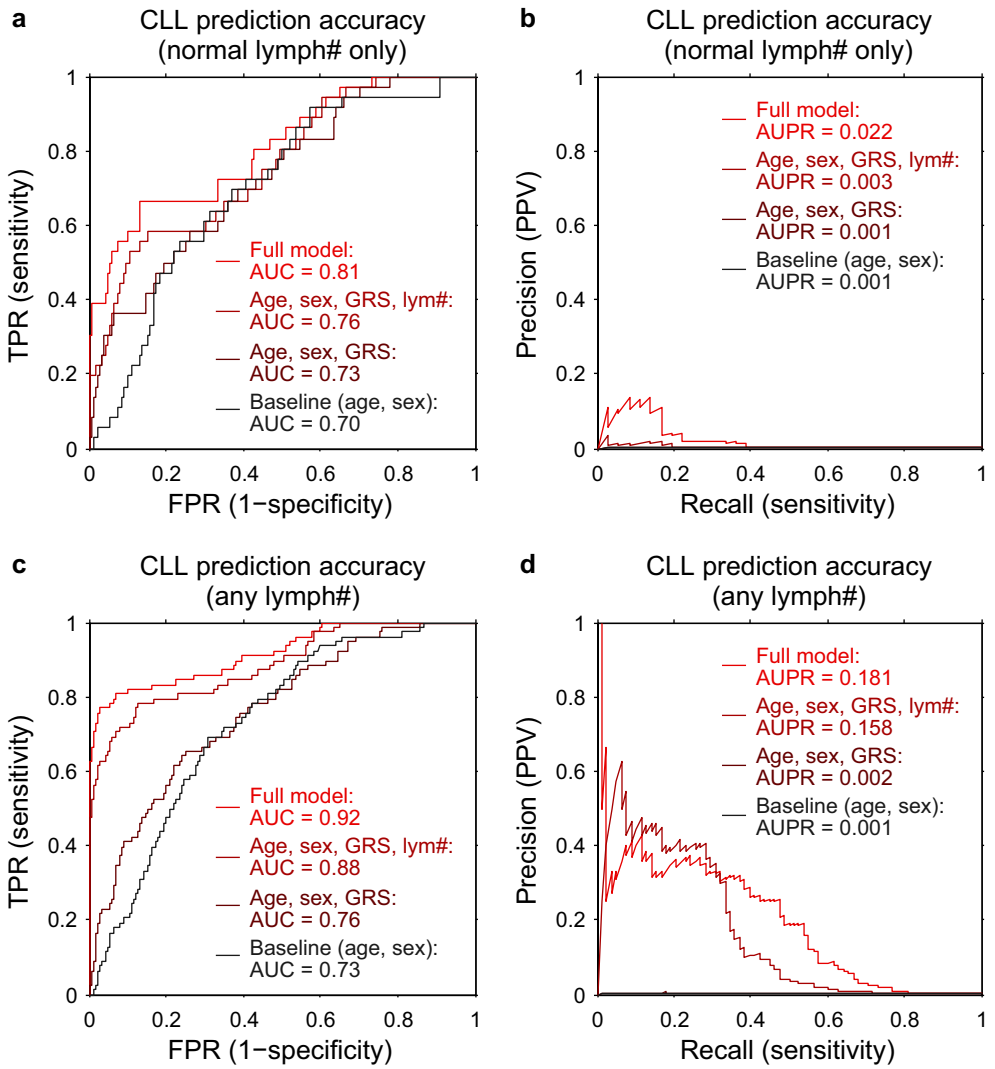

Extended Data Fig. 9 | CLL prediction accuracy: receiver operating curves and precision-recall curves. CLL prediction benchmarks using tenfold stratified cross validation on: only individuals with lymphocyte counts in the normal range (1×10^9/L to 3.5×10^9/L), as in our primary analyses ($n = 36$ cases, 113,923 controls) (**a**, **b**); and individuals with any lymphocyte count ($n = 78$ cases, 118,481 controls) (**c**, **d**). **a** matches Fig. 5b, and **b** shows the precision-recall curve from the same analysis. **c** and **d** correspond to an analogous analysis in which we removed the restriction on lymphocyte count and also used additional mosaic event variables for prediction (11q−, 14q−, 22q−, and total number of autosomal events). In both benchmarks, individuals with previous cancer diagnoses or CLL diagnoses within 1 year of assessment were excluded; however, some individuals with very high lymphocyte counts pass this filter (and probably already had CLL at assessment despite being undiagnosed for more than 1 year), hence the difference in apparent prediction accuracy between the two benchmarks.

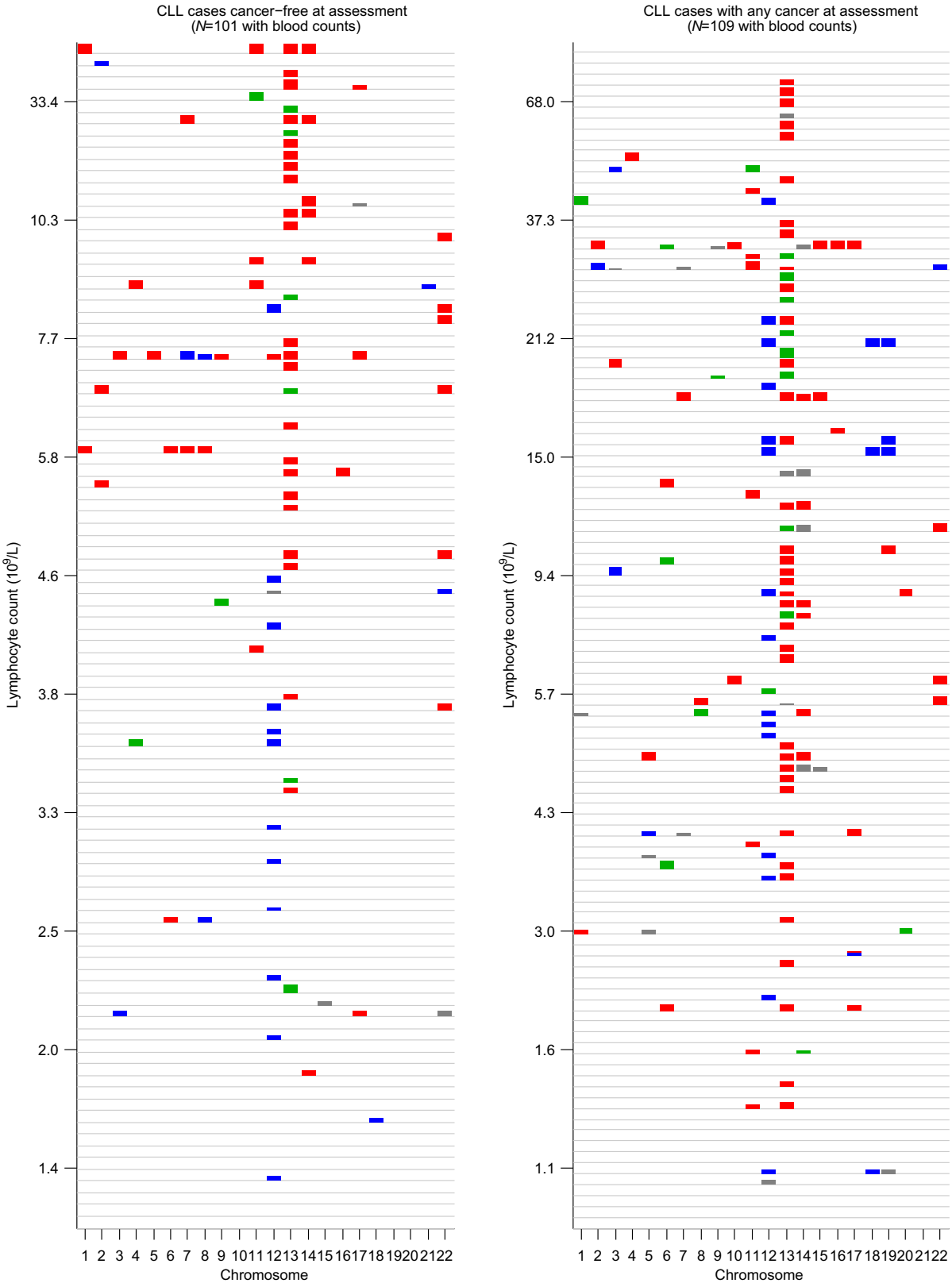

Extended Data Fig. 10 | Mosaic chromosomal alterations detected in CLL cases sorted by lymphocyte count. Individuals are stratified by cancer status at DNA collection (no previous diagnosis versus any previous diagnosis), and mCAs (red, loss; green, CNN-LOH; blue, gain; grey, undetermined) are plotted per chromosome as coloured rectangles (with height increasing with BAF deviation).

nature research

Corresponding author(s): Po-Ru Loh, Giulio Genovese, Steven A. McCarroll, Alkes L. Price

☐ Initial submission ☐ Revised version ☒ Final submission

Life Sciences Reporting Summary

Nature Research wishes to improve the reproducibility of the work that we publish. This form is intended for publication with all accepted life science papers and provides structure for consistency and transparency in reporting. Every life science submission will use this form; some list items might not apply to an individual manuscript, but all fields must be completed for clarity.

For further information on the points included in this form, see Reporting Life Sciences Research. For further information on Nature Research policies, including our data availability policy, see Authors & Referees and the Editorial Policy Checklist.

Experimental design

1. Sample size

Describe how sample size was determined.

We analyzed all samples in the UK Biobank available at the time we began the study (the interim release, ~30% of the full UK Biobank data set). We reasoned that this sample size would be sufficient given (a) the success of previous studies of similar or smaller sizes (e.g., Jacobs et al. 2012, Laurie et al. 2012, Machiela et al. 2015, Vattathil & Scheet 2016) and (b) our new, more sensitive detection methodology.

2. Data exclusions

Describe any data exclusions.

We removed 480 individuals marked for exclusion from genomic analyses based on missingness and heterozygosity filters and 1 individual who had withdrawn consent, leaving 152,248 samples. We further removed 320 samples with median s.d.(BAF)>0.11 indicating low genotype quality. Finally, we removed an additional 725 samples with evidence of possible contamination (based on apparent short interstitial CNN-LOH events in regions of long-range linkage disequilibrium) and 1 sample without phenotype data, leaving 151,202 samples for analysis.

3. Replication

Describe whether the experimental findings were reliably reproduced.

All attempts at replication were successful: we replicated the genetic associations we identified at 10q and 15q, and we replicated our results concerning the age and sex distributions of particular events. Further replication is needed for the other genetic associations we identified (which were too weak allow reasonable replication power) and the associations with blood phenotypes and health outcomes.

4. Randomization

Describe how samples/organisms/participants were allocated into experimental groups.

We did not allocate samples into experimental groups.

5. Blinding

Describe whether the investigators were blinded to group allocation during data collection and/or analysis.

We did not collect samples, and we did not allocate samples into groups.

Note: all studies involving animals and/or human research participants must disclose whether blinding and randomization were used.

6. Statistical parameters

For all figures and tables that use statistical methods, confirm that the following items are present in relevant figure legends (or in the Methods section if additional space is needed).

n/a	Confirmed	
☐	☒	The exact sample size (*n*) for each experimental group/condition, given as a discrete number and unit of measurement (animals, litters, cultures, etc.)
☒	☐	A description of how samples were collected, noting whether measurements were taken from distinct samples or whether the same sample was measured repeatedly
☒	☐	A statement indicating how many times each experiment was replicated
☐	☒	The statistical test(s) used and whether they are one- or two-sided (note: only common tests should be described solely by name; more complex techniques should be described in the Methods section)
☐	☒	A description of any assumptions or corrections, such as an adjustment for multiple comparisons
☐	☒	The test results (e.g. *P* values) given as exact values whenever possible and with confidence intervals noted
☐	☒	A clear description of statistics including central tendency (e.g. median, mean) and variation (e.g. standard deviation, interquartile range)
☐	☒	Clearly defined error bars

See the web collection on statistics for biologists for further resources and guidance.

Software

Policy information about availability of computer code

7. Software

Describe the software used to analyze the data in this study.	We performed genotyping QC and cis association tests using PLINK 1.90, haplotype phasing using Eagle 2.3, heritability estimation and trans association tests using BOLT-REML / BOLT-LMM 2.3, identity-by-descent detection using GERMLINE 1.5.1, and imputation using Minimac3 (1.0.14). We also used custom algorithms described in Methods and the Supplementary Note.

For manuscripts utilizing custom algorithms or software that are central to the paper but not yet described in the published literature, software must be made available to editors and reviewers upon request. We strongly encourage code deposition in a community repository (e.g. GitHub). *Nature Methods* guidance for providing algorithms and software for publication provides further information on this topic.

Materials and reagents

Policy information about availability of materials

8. Materials availability

Indicate whether there are restrictions on availability of unique materials or if these materials are only available for distribution by a for-profit company.	No unique materials were used.

9. Antibodies

Describe the antibodies used and how they were validated for use in the system under study (i.e. assay and species).	No antibodies were used.

10. Eukaryotic cell lines

a. State the source of each eukaryotic cell line used.	No eukaryotic cell lines were used.
b. Describe the method of cell line authentication used.	No eukaryotic cell lines were used.
c. Report whether the cell lines were tested for mycoplasma contamination.	No eukaryotic cell lines were used.
d. If any of the cell lines used are listed in the database of commonly misidentified cell lines maintained by ICLAC, provide a scientific rationale for their use.	No eukaryotic cell lines were used.

Animals and human research participants

Policy information about studies involving animals; when reporting animal research, follow the ARRIVE guidelines

11. Description of research animals

Provide details on animals and/or animal-derived materials used in the study.	No animals were used in the study.

Policy information about studies involving human research participants

12. Description of human research participants

Describe the covariate-relevant population characteristics of the human research participants.	The study did not involve human research participants. (Only previously-collected data from UK Biobank was analyzed.)